NISTIR 7424

Verification of a Gas Mask Calibrant

Robert Fletcher
George Mulholland
Jiann Yang
Lance King
Michael Winchester
Donna Klinedinst
Jennifer Verkouteren
David Buckingham
Thomas Cleary
James Filliben

NISTIR 7424

Verification of a Gas Mask Calibrant

Robert Fletcher[1], George Mulholland[2], Jiann Yang[2]
Lance King[1], Michael Winchester[3], Donna Klinedinst[1], Jennifer Verkouteren[1], David Buckingham[1], Thomas Cleary[2] and James Filliben[4]
[1] Surface and Microanalysis Science Division
[2] Fire Research Division
[3] Analytical Chemistry Division
[4] Statistical Engineering Division
National Institute of Standards and Technology
Gaithersburg, MD 20899

Sponsors

Office of Law Enforcement (OLES)
Alim Fatah and Philip Mattson
National Institute of Standards and Technology
Gaithersburg, MD 20899

U.S. Army/ Calibration Coordination Group (CCG)
D. Greg Boggs
Applied Physics Standards Laboratory
U.S. Army Primary Standards Laboratory
Redstone Arsenal, AL 35898

Executive Summary

The calibrant in the M41 Protection Assessment Test System and the civilian PortaCount test stand, a TSI 3760a condensation particle counter*[*], was calibrated to a NIST-traceable aerosol electrometer. This is the first time aerosol concentration measurements have been made traceable to electrical standards. A second independent method of determining the test aerosol concentration employed in the study was quantitative particle collection by filtration followed by particle counting by electron microscopy. An electrospray aerosol generator was used to produce the monodisperse challenge aerosol. The electrospray eliminated a strong bias in the aerosol electrometer results produced by multiple charging of the test aerosol particles. The data included in this report apply only to the individual instruments tested in this work and should not be generalized to apply to all 3760a condensation particle counters.

Introduction

Military and civilian first responder personnel wear gas masks for protection against chemical, biological, and fire combustion products. The recognized potential world-wide threat from chemical and biological agents and the need for civilian protection demands that effective personal protection equipment be available. An important part of this defense strategy is the testing and verification to assure secure gas mask fit. The M41* shown in Figure 1 was developed to allow the military to field-test its protective equipment on the person using the protective devices.

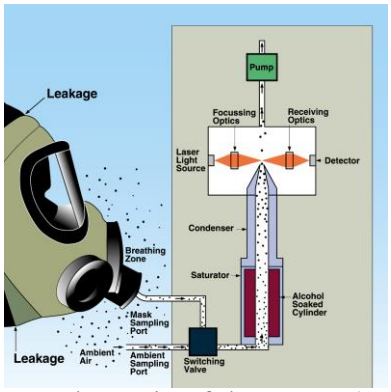

Figure 1. Schematic of the M41. (Courtesy of TSI)

[*] Commercial equipment, instruments, and materials, or software are identified in this report to specify adequately the experimental procedure. Such identification does not imply recommendation or endorsement of these items by the NIST, nor does it imply that they are the best available for the purpose.

The Army determines the gas mask fit quality by measurement and comparison of the ambient aerosol concentration outside of the fitted masks to the aerosol concentration inside. Small aerosol particles are used as surrogate gas test agents because they behave in a similar manner and have nearly the same fluid dynamical properties as the airflow streams of gas agents. The particles can be used to identify both leaks in the mask and inefficiencies in the filter. This technology is believed to provide a complete diagnostic of the integrity of the mask, the filter and the fit on the individual.

The Army, working with TSI, Inc., an aerosol instrument manufacturer, has developed the M41 Protective Assessment Test Systems (PATS) to test and verify M41s (shown in Figure 2). The components of the PATS test stand are an aerosol generator, aerosol electrical charger, a mobility classifier to produce monodisperse 80 nm diameter aerosol, an aerosol dilution system and two condensation particle counters (CPCs). The test aerosol concentration range is 100 particles/cm^3 – 10 000 particles/cm^3. The CPCs serve as the calibrants in the test stand for the M41s.

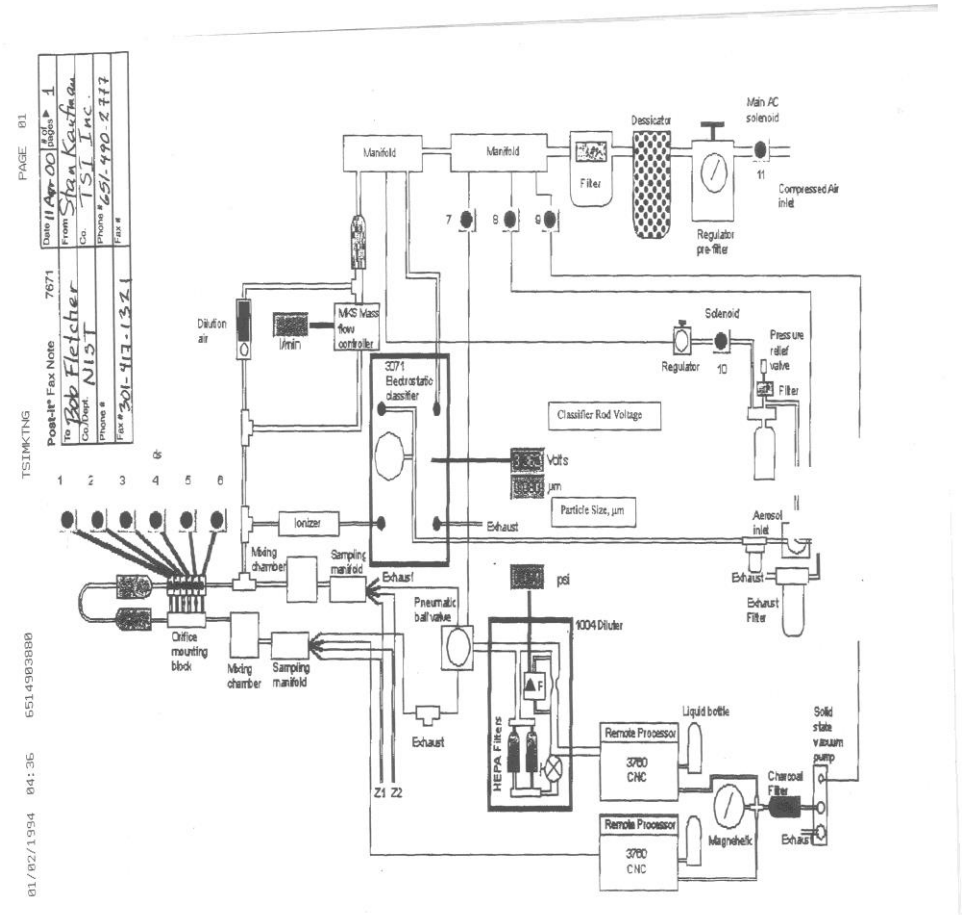

Figure 2. Schematic of the TSI built test stand used to verify M41 performance. (courtesy of TSI)

In the past, the Army has relied on TSI to calibrate the CPCs; TSI uses an aerosol-electrometer (AE) -based instrument to calibrate the CPCs. There are no aerosol concentration standards for the CPCs nor are there certified reference materials available

for aerosol concentration standardization. With present technology and the transient nature of aerosol, a certified reference material for aerosol concentration has not been feasible.

One objective of this work is to provide measurement assurance to the US Army for their gas mask fit-test method by assuring the accuracy of the aerosol concentration measurement integral to this test method. Simultaneously, the civilian first responders also benefit from such verification. The U.S. Army Test, Measurement, and Diagnostic Equipment Activity (USATA) requires the development of an aerosol concentration standard method, traceable to the National Institute of Standards and Technology (NIST). This standard method would enable the calibration of Condensation Particle Counters that are currently used to calibrate M41 PATS for the Army.

Experimental Design and Procedure

The intercomparison of a condensation particle counter (CPC) and an aerosol electrometer (AE) was carried out using nominal 80 nm diameter solid polystyrene latex (PSL) spheres. PSL's were incorporated into the experimental design to help reduce multiple charging of the aerosol. We used a basic test stand design similar to the one shown in Figure 3. The system consists of a Collison aerosol generator, two diffusion dryers and an electrical charge neutralizer to condition the aerosol. Another test stand that we used for tests employed an electrospray aerosol generator. The aerosol was "mobility band pass filtered" using a differential mobility analyzer (DMA) model 3080 made by TSI to produce a monodisperse 80 nm aerosol. The aerosol must be electrically charged to be classified by the DMA.

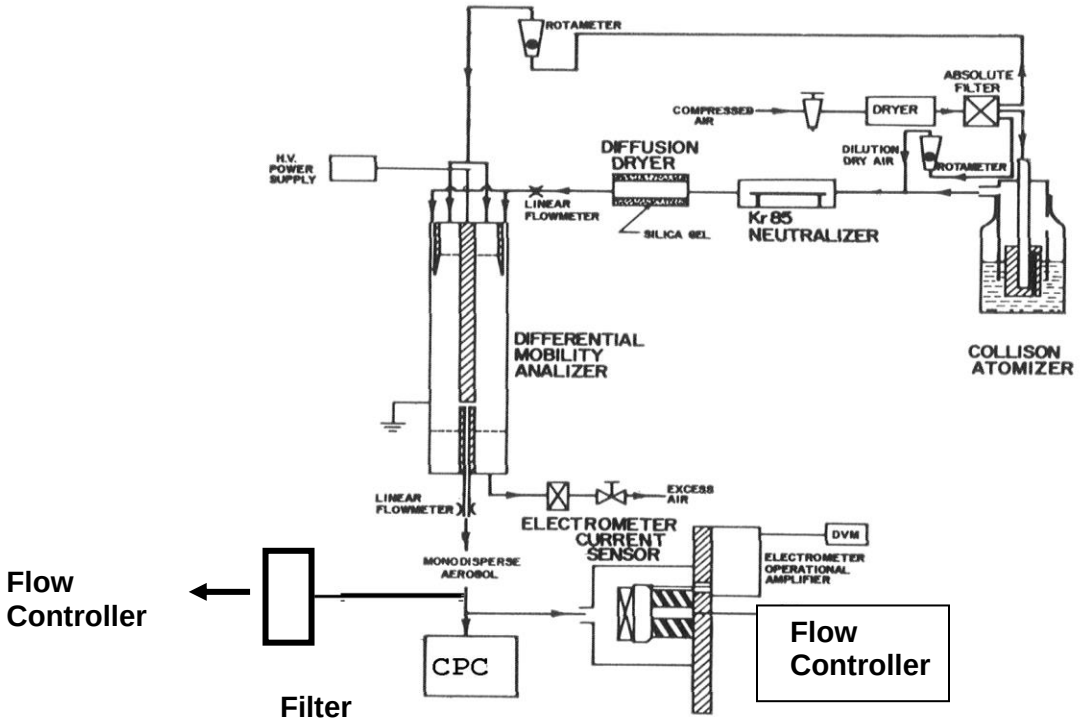

Figure 3. Schematic of experimental apparatus that produces and conditions the aerosol, and the configuration of the CPC, AE and filter. The instruments do not sample simultaneously, but in a sequential fashion. (adapted from Liu and Pui, 1974)

We chose to use monodisperse polystyrene spheres to eliminate or at least minimize multiply charged particles that can be transmitted through the DMA and because we can characterize the spheres by electron microscopy. The particle size was chosen based on the fact that an 80 nm aerosol is used in several test facilities and that the CPC counts nearly 100 % of the particles at this size. We employed a TSI model 3068 aerosol electrometer* (AE) as an independent means of measuring the particle concentration. The AE determines the particle concentration as a function of electrical current that results from the flow of charged particles through this instrument. The AE was calibrated before each use by a femtoampere current source produced from a high precision voltage source and a nominal 100 GΩ resistor. Both the resistor properties and the voltage source were measured by the Electricity Division at NIST. The NIST voltage source had a relative uncertainty (u/V) of 5×10^{-6} and the measurements on the resistor showed the relative uncertainty in the resistance (u_R/R) of $3.5 \times 10.^{-4}$ These measurements permit the measurements of the AE to be traceable to NIST through a traceable current source, which is, in turn, traceable to the volt (Josepheson junction) and the ohm (quantum Hall effect).

The condensation particle counter was a model 3760A which operates only in the single particle count mode. No photometric transition occurs in this instrument. The flow rate is controlled by a critical orifice. The flow rates were determined for both the CPC and AE using a piston displacement meter that was calibrated to the NIST primary standard, the piston prover. The relative uncertainty was approximately 0.008 over the range of the measurements.

Microscopy

In addition, as a second independent measurement approach, we measured the aerosol concentration by quantitative collection of the flowing aerosol onto a filter and counting the number of particles by scanning electron microscopy. The flow rate of the aerosol and the collection duration provide the aerosol volume collected. Polycarbonate filters with a 25 mm diameter and 50 nm pore size were used for these experiments. Since the pore size is approximately 60 % less than the particle diameter, the 80 nm particles are captured with > 99 % efficiency (Green et al., He et al.). The sample was gold-coated in a cold, Ar plasma and mounted in the Hitachi S-4500 field emission scanning electron microscope (SEM). The effective filtration area for particle collection was determined by collecting a large concentration of tungsten oxide particles on the filter. The diameter of the circular area covered by the tungsten particles was measured with a micrometer optical microscopy stage. The PSL spheres are difficult to see by SEM because the low atomic number carbon base spheres are similar in composition to the filter substrate. However, the electron backscatter images of the Au coated spheres are clearly visible as shown in Figure 4.

We randomly selected fields-of-view from the filter surface that included the entire effective sampling area of the filter including edge regions where the particle coverage deceases. Random sampling of the filter surface minimizes uncertainty due to variations in the particle coverage on the sample filter. An SEM magnification of 20 000x produces a field-of-view of approximately 32 μm^2. Images from approximately 25 to 250 fields for each sample were collected and stored for analysis. The number of fields, 250, was chosen by statistical design as a compromise between reducing sampling uncertainty and limiting the number of fields collected. Automated image analysis was not used because in some cases image contrast often gave artifacts so each field was counted by visual inspection. All sample flow rates for the CPC, AE and filter were measured with low uncertainty using a BIOS DryCal flow meter that was verified by the Process Measurements Division at the NIST flow facility. The aerosol concentration is then determined by

$$N = \frac{N_m * A_f}{Q * t_c * A_n} \qquad (1)$$

where N is the aerosol concentration, N_m is the number of particles counted in the SEM fields-of-view, A_f is the effective area of the filter, Q is the flow rate, t_c is the collection time and A_n is the area of the SEM fields-of-view.

The uncertainty in the determination of aerosol concentration by scanning electron microscopy is dependent on (1) particle counting, (2) aerosol flow rate and (3)

the measured surface area of the filter sampled. To assure accurate area determination for each field-of-view, we determined the variation in measured area as a function of SEM stage height. We used the NIST SRM 484g SEM pitch standard to calibrate the image field area at each height and between each filter measurement. Using SRM 484g as the length standard and varying the SEM stage height from 5 mm to 30 mm, we found that the length change was approximately 2 nm/mm of height. We made all of our measurements at a constant stage height of 15 mm. Even for a height variation of 1 mm, there would be minimal contribution of only ≈ 4 nm^2 to the area compared to the entire field-of-view area that is approximately 3.2×10^7 nm.^{2} The effect is negligible compared to the other uncertainty components. The components contributing to the measurement uncertainty will be covered below in the results discussion.

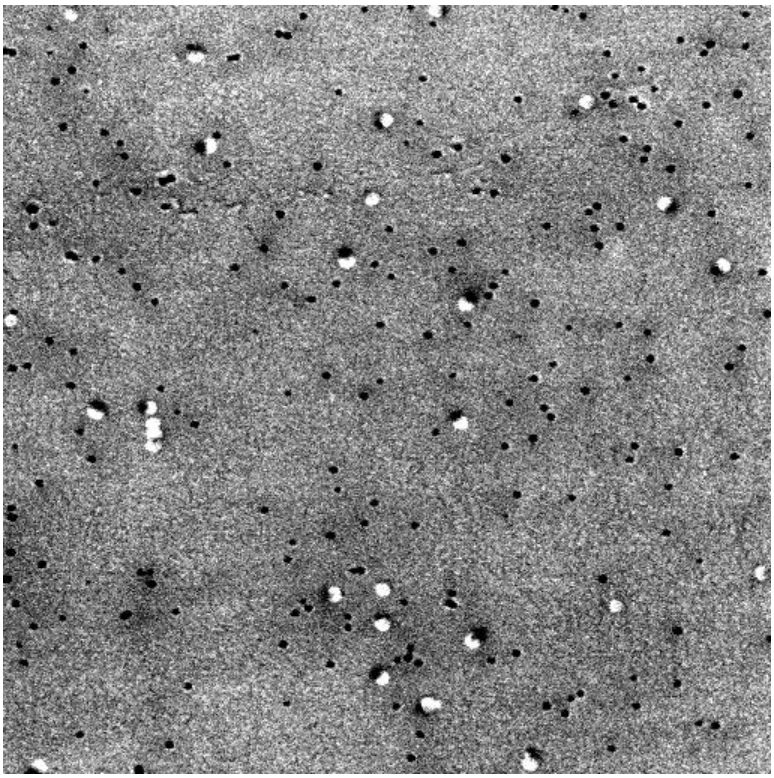

Figure 4. SEM backscatter image of polystyrene spheres on polycarbonate filter. The spheres appear as lighter shaded circular objects.

Collison Nebulizer Experiments

Eighty nanometer PSL aerosol is produced using the Collison nebulizer operating at approximately 206.86 kPa (30 psi). Five particle suspensions are used that provide aerosol concentrations ranging from approximately 150 particles/cm^3 to 13 000 particles/cm^3. The DMA voltage is scanned to locate the single-charged (singlet) monomer 80 nm particle population. An example of such a scan is shown in Figure 5.

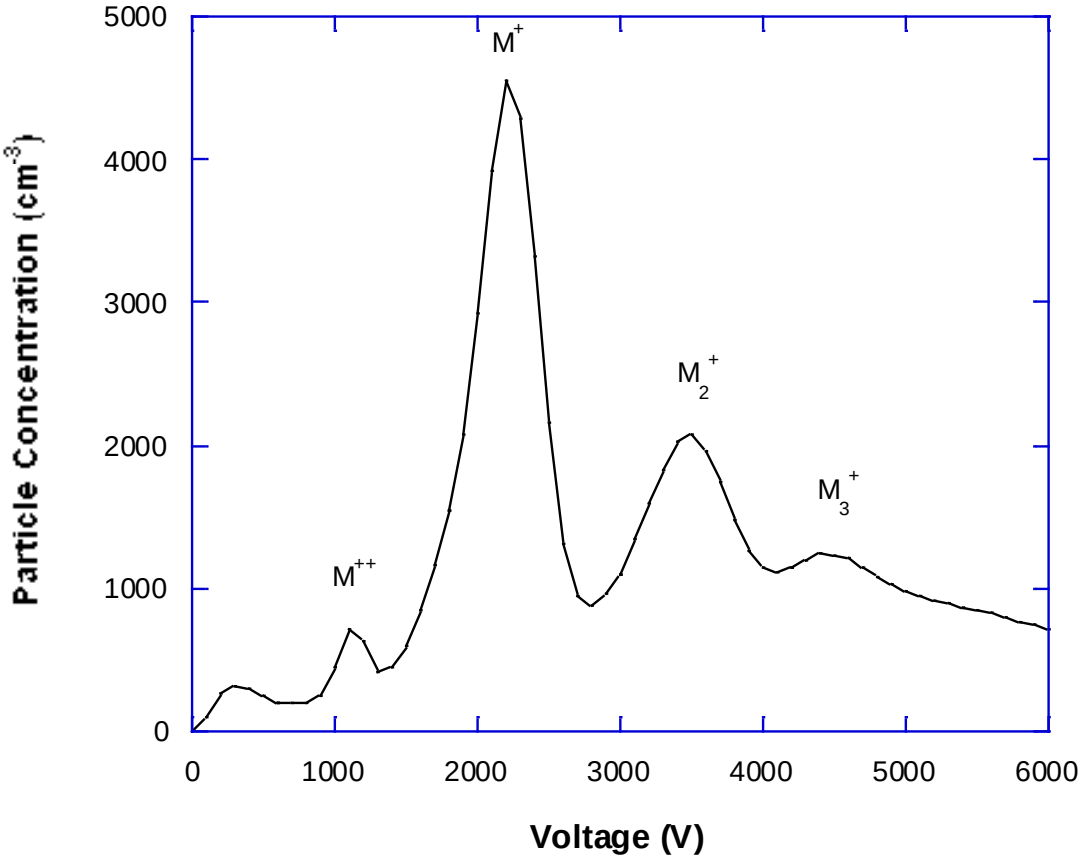

Figure 5. DMA voltage scan of 80 nm polystyrene spheres nebulized from water suspension. M^{++}, M^{+}, $M_2^{+}$and M_3^{+} are the doubly charged monomer peak, the singlet monomer peak, the singlet dimer peak, and singlet triplet, respectively.

The large peak is the singlet 80 nm monomer particle contribution. The small peak at approximately 1000V is the doublet monomer and the broad peak at 3300 V is the singlet dimer. The DMA is operated using the voltage (approximately 2000 V) and flow rates associated with transmission of the singlet 80 nm monomer particle. The CPC and AE are sequentially challenged with the aerosol being produced. The concentration data from each instrument is stored through independent computer interfaces. A clean air blank is recorded (void of aerosol) that passes through the entire system including the DMA. This blank is different from the zero obtained in the electronic calibration. Each day, the particle suspensions were randomly selected to avoid any systematic sampling bias that might result from a sequential process. For the last suspension, a filter housed in a sealed metal filter holder was used to quantitatively collect the aerosol for a known time period to use in the microscopy determination of concentration. Flow rates for all instruments are measured with the same traceable flow rate calibrant as well as for the filter sample.

The procedure for taking the CPC – AE comparison measurements is as follows: An electrode is installed into the AE replacing the aerosol filter, all electronics (including voltage source), CPC, DMA are turned on, cables are adjusted and the instrument allowed to stabilize for up to 24 h. Low femtoampere current measurements require this

stabilization time. Test currents over the range of 0 fA to 150 fA are applied through the electrode assembly to the AE and the response voltage from the electrometer is recorded. It is important to note that this set of measurements electronically calibrates the entire AE-data acquisition system from the electrometer to the computer data collection. The electrode is removed and the filter is reassembled on the AE. The final calibration is given in the discussion of the results.

Electrospray Aerosol Generation

A commercial electrospray aerosol generator operating with a 40 μm diameter capillary was used to produce the PSL aerosol. Suspensions were made of 1 drop to 3 drops of 80 nm PSL (nominal 1% solid spheres) per 1mL of ammonium acetate solution. Experiments were designed to be conducted over 5 days. Each day an AE calibration was performed and 5 aerosol concentrations of the 80 nm PSL produced from the electrospray aerosol generator were used to calibrate the CPC. For each day, two of the aerosol concentrations, 500 cm^{-3} and 5000 cm^{-3} were always produced to measure day-to-day variability. The other 3 concentrations were chosen to be in the range of 100 cm^{-3} to 12 000 cm^{-3}. As shown in Figure 6, a low flow rate CPC was operated to sample the aerosol continuously over the experimental time frame. Data from this instrument was useful to identify fluctuations or variations in the output of the aerosol generator. Each instrument was exposed to the test aerosol at a specified concentration for at least 300 s after the instrument readings stabilized. There were approximately 50 individual readings recorded during the test period.

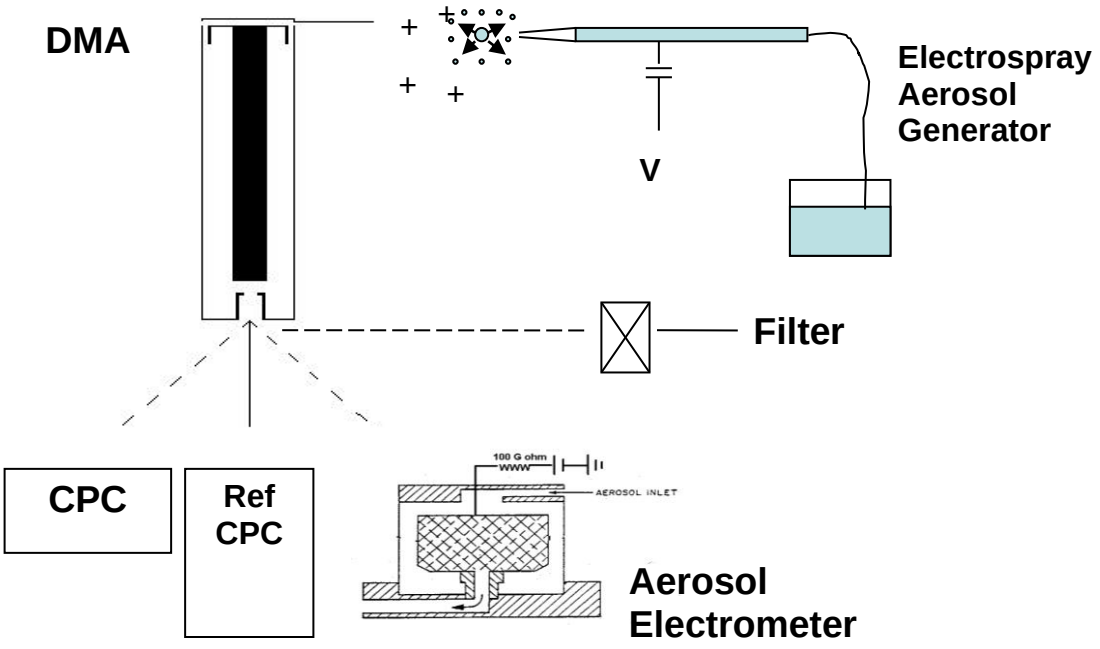

Figure 6. Schematic of test stand used to compare the test CPC and AE. A low sample volume reference CPC was operated through out the experiments and filter was collected for certain aerosol concentrations.

Results and Discussion:

Aerosol Electrometer Calibration

We calibrated the AE immediately before conducting each experiment to compare the AE and CPC with test aerosol. The combined data is shown in Figure 7 for 5 data sets taken over 4 days spanning several weeks. A linear least square regression to the data provides the relation of the voltage response of the electrometer to the applied current. The relation in terms of current, I and voltage, V, is

$$V = -3.02 \times 10^{-5} + 9.8163 \times 10^{11} I \qquad (2)$$

The intercept represents a voltage offset. To reduce the aerosol data, the operating zero was found for the electrometer by sampling particle and charge free air. This voltage offset was subtracted from the measured voltage found from an aerosol population.

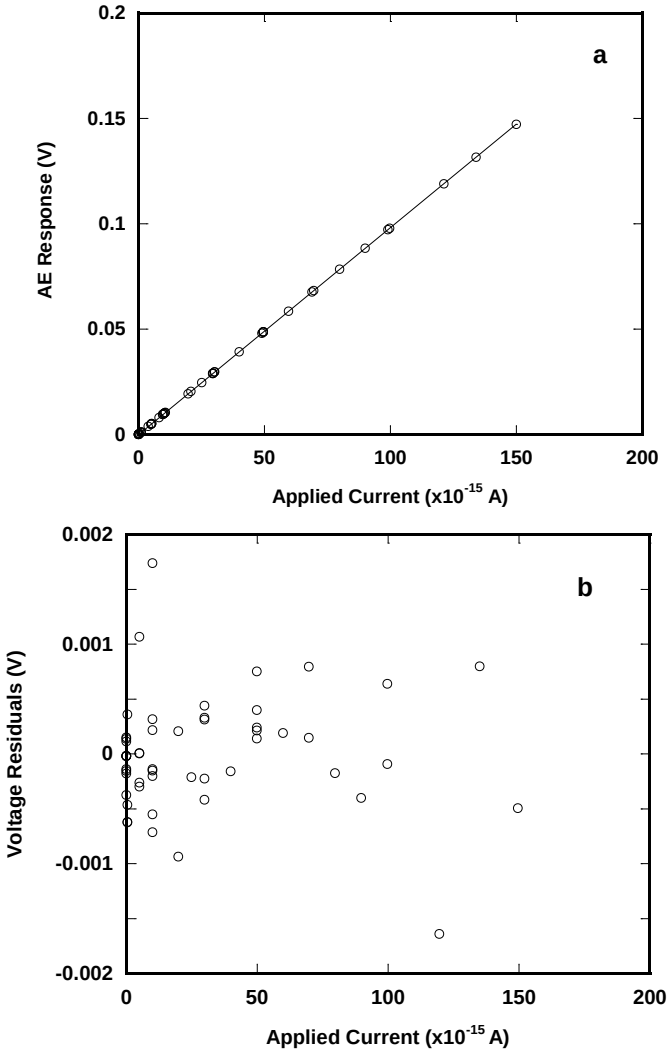

Figure 7. Calibration curve of standardized applied current and AE voltage response (a) and the voltage residual plot (b).

The 67% confidence interval for this regressed line was obtained and the uncertainty in the current is found to be 0.107 x 10^{-15} A (Snedecor and Cochran, 1967). It is also seen from Figure 7b that the distribution of the residuals is independent of the applied current.

AE-CPC Results

A response curve comparison of the CPC and AE are shown in Figure 8 for the Collison nebulizer test facility. These results reflect many measurements over different days where each day the AE was calibrated using the method described above before the AE-CPC comparison was run. The aerosol current was derived from the measured AE response voltage and the application of the AE current-voltage calibration. The blank for the AE calibration was the voltage for particle free and charge free air that was accomplished by passing only clean air through the test stand and the AE. The zero voltage values are possibly affected by residual charged air molecules and are slightly different from the electrically determined zero voltage from the circuit calibration procedure. The calibration curve (equation 2) is used to convert the voltage reading from the AE to current values and then to aerosol concentration through the equation

$$N = \frac{I}{Qe} \qquad (3)$$

where N is the aerosol concentration, I is the current, Q is the flow rate and e = 1.6021 x10^{-19} C is the magnitude of the elementary charge. The aerosol concentrations are not exactly the same from day-to-day, but the same aerosol population produced during that measurement session challenges each instrument.

The results for the Collison nebulizer generating 80 nm test aerosol is shown in Figure 8. It is apparent that the CPC under counts with regard to the AE. There are several explanations for this difference. One, the CPC exhibits coincidence counting, i.e., counts multiple particles as one particle and this becomes increasingly important as the aerosol concentration increases. This coincidence counting error can be as large as 11% at 10 000 particles/cm^3. But at the same time, the AE current becomes more robust as the charged particle concentration (i.e., charge carriers) increases.

The other explanation suggests a bias due to multiple charges on agglomerated particles. The microscopy shows the presence of agglomerated particles. The experiment was designed to eliminate this charge effect, but the SEM images show the presence of a small number of agglomerated particles. The DMA should filter double, triple and larger agglomerates from the transmitted aerosol because we are operating on the mode of the single charged, monomer 80 nm particle peak in the mobility scan. For an agglomerate to get through the DMA, it must have the same electrical mobility as the single particle. The only way for it to attain this mobility is by multi-charging. Agglomerates and single 80 nm particles are counted each as individual particles in the CPC. Since the AE counts charges, this individual particle would not be counted as the CPC does (as one particle), but as multiple particles. The bias in the CPC-AE data most likely results from multiple charging of the PSL agglomerates.

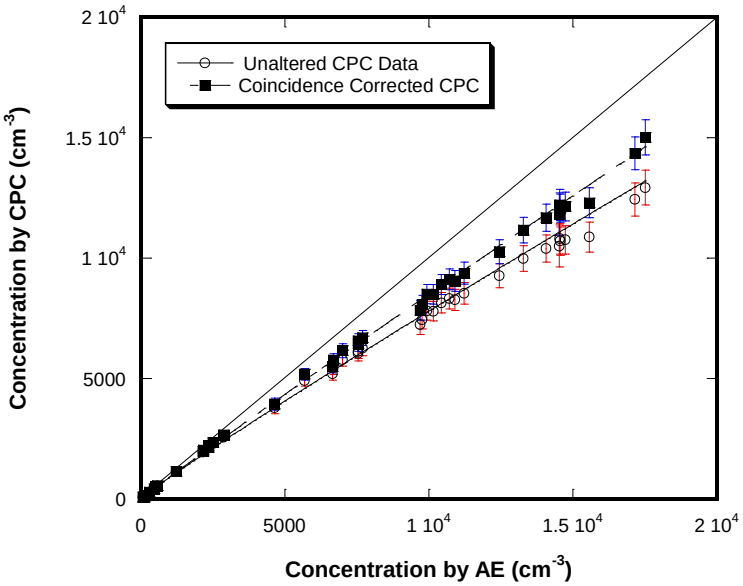

Figure 8. Comparison of AE and CPC responses to the same 80 nm aerosol population produced from the Collison nebulizer. The unmodified data (open circles) and the coincidence counting correction to the CPC (solid squares). Line is a 1:1 relation for reference and the uncertainty is the standard deviation in the mean. The data is exponentially fitted.

Coincidence Effect on the CPC Counting

In optical particle counting it is possible to have two particles in the sensing volume at the same time, especially at high particle concentrations. In this case, the light scattering signal will be interpreted as one particle with an amplitude larger than the individual particles. This reduction in measured particle count as a function of increased particle concentration is referred to as the coincidence counting effect.

In analyzing the coincidence effect, it is helpful to think in terms of the time dependent scattering signal of a particle as it enters the light beam. Once the light scattering from a single particle exceeds a threshold value, its time history will be tracked. The light scattering signal will increase as it traverses the more intense region of the Gaussian beam until it reaches a peak value. Near the time of peak intensity, the electrical signal is processed to allow time for the signal to be read by the electronic processor. During this counting time, t_c, which includes the transit time and the process time, the presence of a new particle will not be counted as a second particle.

As discussed by Gebhart (2001), there are various options in terms of the electronic configuration of the detector. The coincidence effect can be expressed as a ratio of the measured number concentration, N_m, to the number concentration, N. An approximate equation for describing the coincidence effect for less than a 10 % loss in particle counts is given in terms of the volumetric flow rate Q and the counting time t_c by (Gebhart):

$$\frac{N_m}{N} = \exp(-NQt_c) \quad \text{or} \quad \frac{N}{N_m} = \exp(NQt_c) \qquad (4)$$

The effective time that the particle is in the scattering volume for the CPC in our experiments is about 0.4 μs (TSI manual) and Q is determined empirically in our experiments. Even after the application of the manufacturer's recommended coincidence correction, there is still approximately 12% to 15% unaccounted for deviation between the CPC and the AE values at high concentrations.

We hypothesize that the approximate 15% bias is due to extra charges carried by the spheres. If the aerosol contains a fraction of multiply charged spheres, then the AE will over report the concentration. The CPC will measure the sphere population independent of charge. The experiment was designed to eliminate larger particles that have the same electrical mobility as 80 nm particles by carrying extra charges. That was a key reason to use 80 nm PSL spheres instead of nebulizing solutions and producing a polydisperse aerosol. The microscopy suggests how the spheres can be more highly charged. In Figure 9, it is evident that there are agglomerated particles. Given the particle coverage density on the filter surface, it is unlikely that these spheres came together on the filter surface- they existed in the aerosol. To pass the 80 nm electrical mobility discriminator (the DMA) these agglomerated particles had to be multi charged. From the mobility of the M_3^+ in Figure 5, we can calculate the expected mobility of M_3^{++} to be 4400 V/2 = 2200 V which over lays the monomer peak. Likewise, the doublet dimer has a mobility of approximately 1800 V, but this is a broad peak and contributions from the right side will presumably also contribute to the monomer 80 nm peak. The microscopy supports the extra charge agglomerated particle hypothesis.

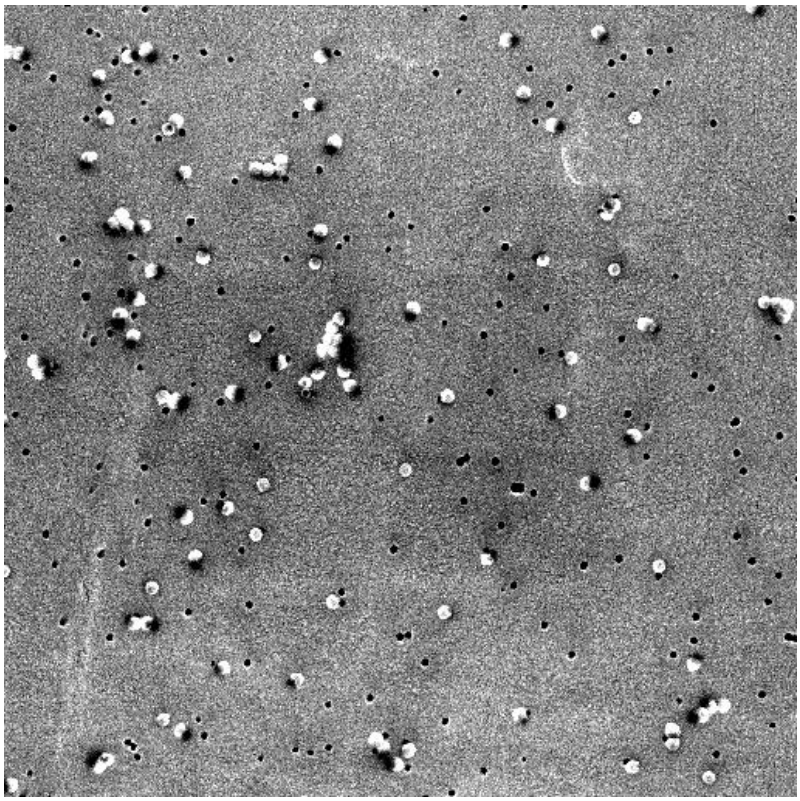

Figure 9. SEM micrograph of 80 nm PSL spheres that have the same electrical mobility as the single 80 nm spheres.

Agglomerated particles are most likely being produced from the Collison nebulizer for the higher concentration PSL liquid suspensions. In this system, the relatively large diameter droplet population increases the probability that more than one PSL resides in some of the drops and consequently upon drying forms a PSL cluster (Liu 2005). It is also evident from Figure 5 that there is a relatively large percentage of singlet dimer and singlet trimer PSL particles. Once again, the electrical mobility of a doublet dimer and doublet trimer particle are very nearly that of the singlet monomer PSL particle. So presumably the multi-charged clusters will not be effectively discriminated from the admitted test aerosol. To minimize agglomeration, several aerosol generators were employed, but none of them were satisfactory. The JR Aerosolizer proved to be very stable, but produced only low aerosol concentrations. With the Laskin nozzle we were also able to get low aerosol concentrations even with high concentration 80 nm PSL aqueous suspensions. A sonic nozzle was tested that could provide high aerosol concentrations, but mimicked the Collison nebulizer in terms of apparent multi-charged particles.

NaCl Aerosol

As an ancillary test of multi charging hypothesis, a 1% by weight NaCl-water solution was nebulized, mobility classified to produce solid 80 nm particles as a

challenge to the CPC and AE. For this system we expect a polydisperse aerosol that is electrically mobility classified in a manner such that some particles will be physically large enough to obtain the 80 nm mobility by carrying multiple charges. The results of this comparison are shown in Figure 10.

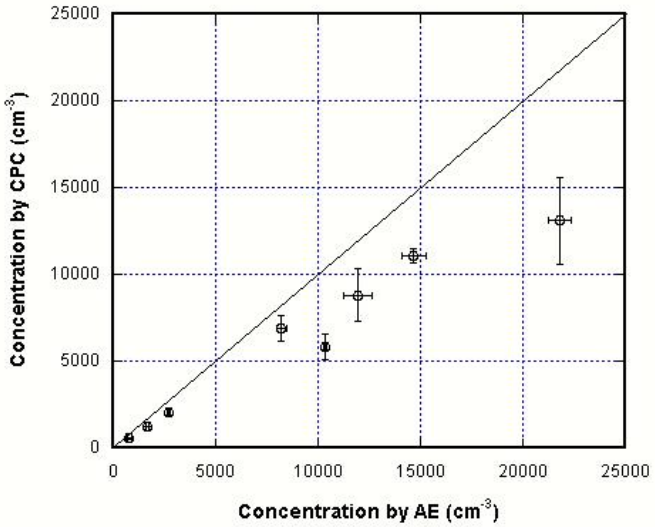

Figure 10. Plot of NaCl aerosol concentration determined by CPC and AE. The data is uncorrected for charge and coincidence. Error bars correspond to standard deviation in the measurements.

Multiple charging will occur with this NaCl polydisperse aerosol. The AE data were corrected for multiple charge by applying a factor of 0.86 (Liu and Pui, 1974) and for coincidence counting in the CPC using equation 4 (above). The corrected plot, Figure 11, shows close agreement between the two instruments for NaCl aerosol.

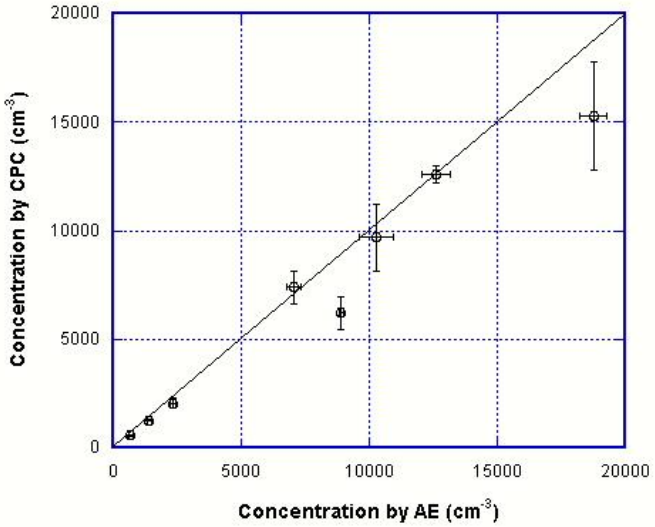

Figure 11. Plot of NaCl aerosol concentration determined by CPC and AE. The AE data are corrected for multiple charge and the CPC data are corrected for coincidence counting. Error bars correspond to standard deviation in the measurements.

AE-CPC Comparison Using Electrospray Aerosol Generator

Osmondson and Sem (2004) recommended the electrospray aerosol generator as a possible method to reduce clustering of the PSL spheres. The electrospray method produces aerosol concentrations from 100 cm^{-3} to approximately 17 000 cm^{-3} with less than 0.5 % single charged doublets and thus presumably much lower percentage of doubly charged doublets. A typical voltage scan by the DMA of aerosol from the electrospray is shown in Figure 12 illustrating the lack of clustered spheres. For example, the concentration of singlet dimers is approximately 0.3 % of the singlet monomers.

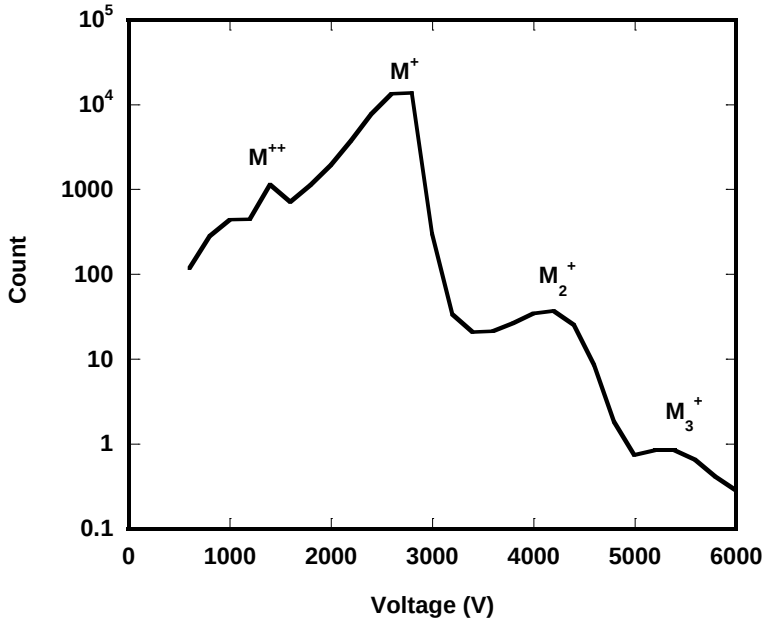

Figure12. DMA Voltage scan of aerosol produced by the electrospray aerosol generator. The plot shows monomer and dimer populations on a semi-log scale.

Figure 13 shows a plot of the aerosol concentration data found for the AE and CPC comparison. Each point represents a mean value with at least 50 individual measurements. The CPC data has been normalized with the ratio of the mean concentrations of the continuous CPC monitor for the periods of the AE data collection and the CPC data collection. Also, an accurate experimentally measured flow rate, approximately 1.41 L/min, was used instead of the nominal 1.5 L/min provided by the manufacturer. The regression will be different for the nominal flow rate.

The linear least squares fit of the log of the concentration found by the CPC versus the log of the concentration found by the AE gives

$$\log(N_{CPC}) = 0.114463 + 0.957427 \times \log(N_{AE}) \text{ or } N_{CPC} = 1.3016 N_{AE}^{(0.957427)} \quad (5)$$

where N_{CPC} and N_{AE} are the aerosol concentrations determined by the CPC and by the AE, respectively. There is no coincidence correction applied to this data. The uncertainty in N_{AE} from the regression at the 67 % confidence interval is 1.01 $cm.^{-3}$ A linear plot of the same data is shown in Figure 14.

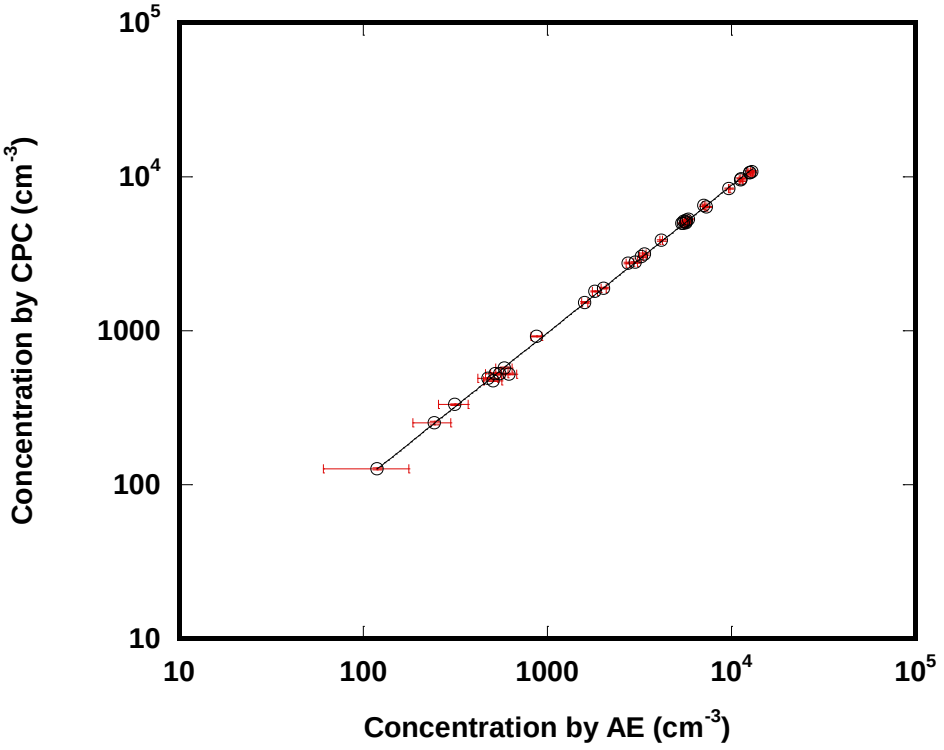

Figure 13. Plot of AE to CPC comparison for original uncorrected CPC data. The fit is per equation 5. The uncertainty bars represent the expanded uncertainty (k=2) associated with AE calibration, flow rate and particle counting.

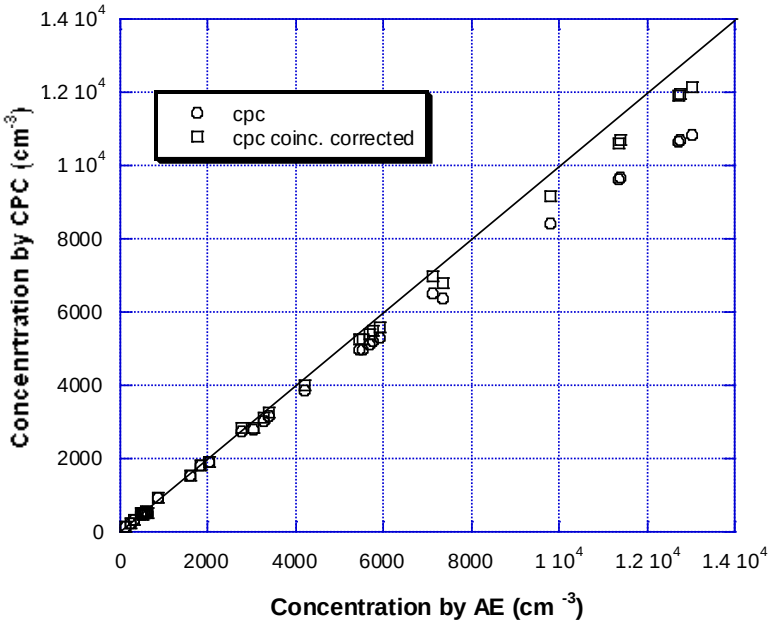

Figure 14. Measured concentrations by CPC and AE plotted on a linear scale including uncorrected data (circles) and coincidence counting corrected points (squares). Line is a 1:1 correspondence.

Even with the manufacturer's recommended coincidence correction for the CPC values, there is still a small deviation from perfect agreement between the two techniques. One explanation is that there is no electronic dead time factored into the correction and that the manufacture's estimated parameters for the coincidence correction are an average; there may be variations from instrument to instrument. However, most importantly, the strong charge bias effect that was on the order of 12 % to 15 % has been effectively eliminated by using the electrospray aerosol generator. Table 1 contains the AE-CPC comparison data with the expanded uncertainty, i.e., twice the combined uncertainty calculated by the method of the square root of the sum of the squared components (k=2; Taylor and Kuyatt, 1994) for the AE measurements. The factor of two would correspond for a normal distribution to be approximately the 95 % confidence interval. The uncertainty includes the uncertainty in the CPC – AE log-linear regression as well as the propagated uncertainties from the current-voltage calibration, variance in both the voltage measurements and the background and the total uncertainty associated with the flow rate or air volume. The concentrations by the CPC are presented for the coincidence uncorrected and corrected data.

Table 1. Data used to construct plots in Figures 13 and 14.

Concentration by AE (cm^{-3})	Expanded Uncertainty in AE Concentration (cm^{-3})	Concentration by CPC no correction (cm^{-3})	Concentration by CPC coincidence corrected (cm^{-3})
478.4	61	490.7	493.0
11306	79	9671.4	10699
5481.8	66	4990.1	5243.4
1601.2	61	1527.4	1549.9
242.74	60	252.05	252.65
583.8	62	575.5	578.6
314.35	64	332	333.0
5385.4	69	5001.1	5253.1
2750.1	126	2756.0	2829.9
7072.5	95	6517.0	6955.2
551.3	63	525.4	528.0
874.2	85	919.7	927.7
2025.9	63	1895.1	1929.8
3373.2	71	3151.7	3249.6
5719.6	72	5216.7	5493.5
5649.4	70	5045.7	5303.9
5516.4	69	5130.4	5397.7
621.7	62	524.6	527.2
119.2	62	127.16	127.3
5863.4	69	5314.6	5600.5
12604	195	10646	11899
3011.4	65	2783.8	2859.3
521.5	63	527.46	530.1
5646.1	87	5122.2	5388.5
9723.8	82	8422.3	9181.5
12628	99	10682	11951
3241.8	70	3033.8	3124.3
4155.2	68	3871.9	4019.4
508.7	62	474.9	477
1816.1	71	1805.4	1836.5
11258	157	9608.6	10603
12904	93	10851	12147
7291.1	73	6376.6	6792.2

Particle Concentration by Microscopy

For selected experiments, the aerosol concentration was determined by microscopy. Figures 15 and 16 provide an overview of the comparison between microscopy data and AE and CPC data. In both plots a line is drawn to indicate the 1:1 relationship between the concentration determined by microscopy and the other measurement technique. SEM microscopy was very beneficial because it uncovered a potential bias with the AE measurement. We observed that the 80 nm PSL were agglomerated in some images. A regression of the concentration determined by the CPC

versus the concentration determined by microscopy, N_{mic}, (Figure 16) for CPC uncorrected coincidence counting is

$$N_{CPC} = 1.66953 N_{mic}^{\,0.931932} \qquad (6)$$

and for coincidence corrected CPC values

$$N_{CPC} = 1.51605 N_{mic}^{\,0.954519} \qquad (7)$$

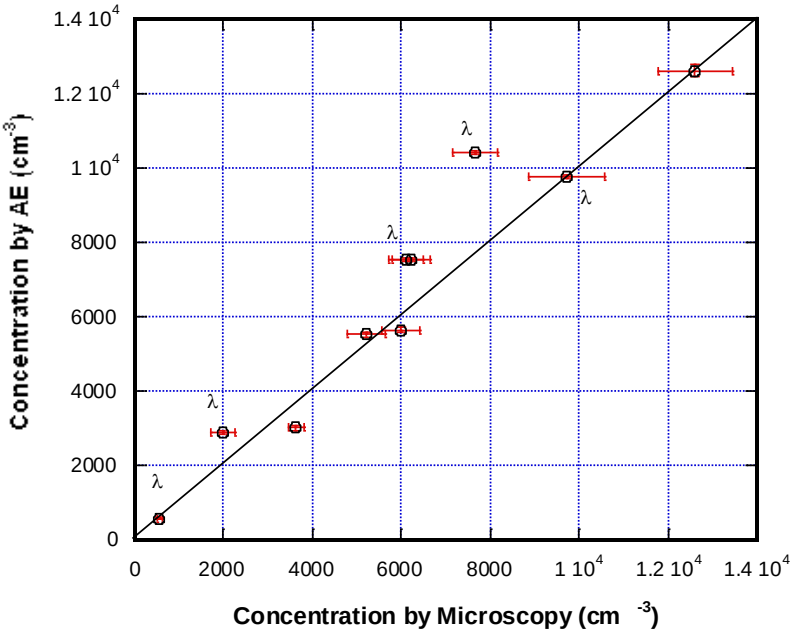

Figure 15. Comparison of the aerosol concentration determined by microscopy and AE where λ denotes counts determined for agglomerated particles. The uncertainty bars correspond to the expanded uncertainty. The data (two points) at approximately 6000 cm^{-3} corresponds to the concentration derived from two independent sets of images collected on the same filter. A 1:1 line is drawn for comparison.

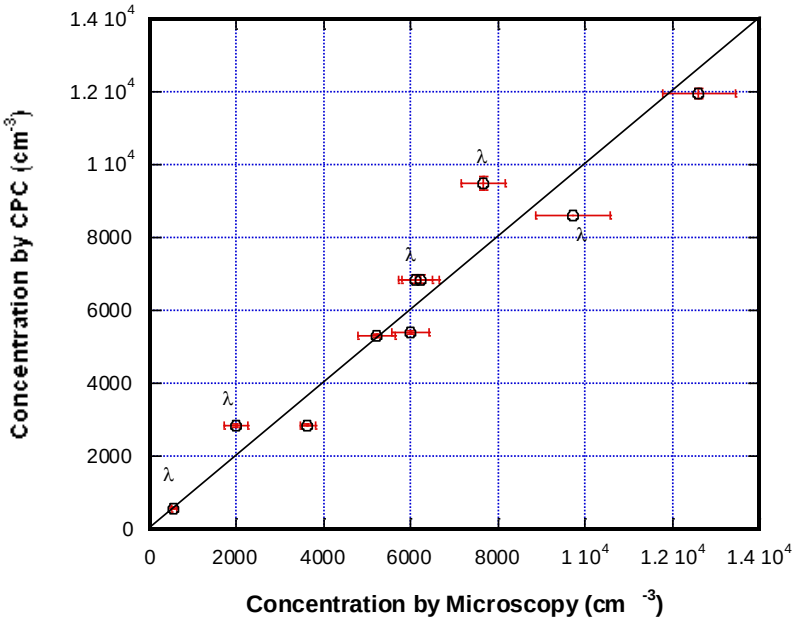

Figure 16. Comparison of the aerosol concentration determined by microscopy and CPC (coincidence corrected) where λ denotes counts determined for agglomerated particles. The uncertainty bars correspond to the expanded uncertainty. The 1:1 line is presented for comparison and is not a fit to the data.

Uncertainties

Uncertainties associated with the AE measurements result from uncertainties in the voltage-current calibration of the AE, the flow rate of aerosol through the sensor and the variance in the voltage measurement and the voltage background. From equation 3, the uncertainty in the aerosol concentration, u_N, is presented in equation 8 (Taylor and Kuyatt, 1994, page 8). The uncertainty in the concentration is expressed as the rate of change with respect to the current, I, the flow rate, Q, and the charge on an electron, e.

$$\frac{u_N}{N} = \frac{\left[\left(\frac{\partial N}{\partial I}u_I\right)^2 + \left(\frac{\partial N}{\partial Q}u_Q\right)^2 + \left(\frac{\partial N}{\partial e}u_e\right)^2\right]^{1/2}}{N} \qquad (8)$$

Which becomes

$$\frac{u_N}{N} = \left[\left(\frac{u_I}{I}\right)^2 + \left(\frac{u_Q}{Q}\right)^2 + \left(\frac{u_e}{e}\right)^2\right]^{1/2}. \qquad (9)$$

A detailed listing of the relative uncertainty components is shown in Table 2. In Table 2, the V-I calibration is the relative uncertainty associated with the voltage-current calibration curve at each concentration (for example, at 5000 particles/cm^3, $0.107x10^{-15}$ A / $20.5x10^{-15}$ A = 0.005), the voltage variability is a random, type A uncertainty that includes the AE measurement voltage and the background voltage summed by taking the square root of the sum of the squares of the respective standard uncertainty in the means. The uncertainty in the measured flow rate includes 3 components. The first is the uncertainty obtained in the calibration of the transfer standard to the primary NIST standard (0.11 %), the second is the uncertainty found by regressing the test meter data to that of the transfer standard flow meter (0.085 %) and the third is the flow rate variability uncertainty in the mean (n=50) for the test meter (type A).

Table 2. Examples of the relative uncertainties associated with the various components contributing to the total uncertainty in the aerosol concentration determined by the AE.

	Uncertainty in Current u_I		Uncertainty in Flow Rate u_Q		
Nominal Concentration (cm^{-3})	V-I calibration	Voltage Variability	Flow Rate NIST	Flow Rate Test Meter	Flow Rate Variability
120	0.24	0.09	0.0011	0.000 85	0.000 17
500	0.05	0.02	0.0011	0.000 85	0.000 18
3000	0.009	0.006	0.0011	0.000 85	0.000 16
5000	0.005	0.003	0.0011	0.000 85	0.000 11
12000	0.002	0.002	0.0011	0.000 85	0.0000 1

The uncertainties are summed in a manner expressed by equation 9 where the last term, u_e, is negligible. The results are shown in Table 3.

Table 3. The combined standard relative uncertainties for the aerosol concentration determination by the AE.

Nominal Concentration (cm^{-3})	Uncertainty in Current u_I/I	Uncertainty in Flow Rate u_Q/Q	Combined Uncertainty u_N/N
120	0.26	0.0014	0.26
500	0.057	0.0014	0.057
3000	0.011	0.0014	0.011
5000	0.0058	0.0014	0.0060
12 000	0.0032	0.0014	0.0035

The combined uncertainty for all of the AE data is shown in Figure 17. The relative uncertainty is high (approximately 26 %) for values at low current (low particle concentration) domains.

Total Uncertainty

The total uncertainty in the CPC measurements are not known, however some components are known and quantified. One source of uncertainty is fluctuation in the aerosol source. An effort was made to normalize this fluctuation by using the reference continuous monitoring CPC that acquired measurements across both instrument sampling periods. Only the type A uncertainties are known for the number of particle counted, N_p, the flow rate, Q_{CPC}, and the ratio of the continuous monitor CPC values for the periods when the AE was sampling and when the test CPC was sampling, f. Also, there is an uncertainty (u_{fit}) associated with the fit of the CPC-AE values given above. We believe this fit uncertainty is correlated with the components described above. The aerosol concentration is

$$N_{CPC} = \frac{f * N_p}{Q_{CPC}}. \qquad (10)$$

Following the analysis method found in equation 9, the relative uncertainty in the concentration found by the CPC, u_{CPC}, is

$$\frac{u_{CPC}}{N_{CPC}} = \left[\left(\frac{u_{Np}}{N_p} \right)^2 + \left(\frac{u_{Q_{CPC}}}{Q_{CPC}} \right)^2 + \left(\frac{u_f}{f} \right)^2 \right]^{1/2}. \qquad (11)$$

Table 4. Typical values for the relative uncertainty including the uncertainty obtained in the AE-CPC fit and the combined uncertainty in the concentration measurements determined by the CPC.

Nominal Concentration	u_{Np}/Np	u_{QCPC}/Q_{CPC}	u_f/f	u_{fit}/N_{CPC}
120	0.0027	0.0014	0.0074	0.0040
500	0.0020	0.0014	0.0041	0.000 97
3000	0.0029	0.0014	0.0045	0.000 17
5000	0.0022	0.0014	0.0032	0.000 10
12000	0.0019	0.0014	0.0066	0.000 052

Knowing the magnitude of the type A uncertainties in the CPC concentration, we can relate this uncertainty to the uncertainty in the AE measurements by the relationship of the CPC and AE found in equation 5 represented by

$$N_{AE} = cN_{CPC}^{\ d} \quad \text{where d = 1.01897} \qquad (12)$$

and

$$\frac{u_{AE}(CPC)}{N_{AE}} = d * \frac{u_{CPC}}{N_{CPC}}. \qquad (13)$$

We are taking the fit uncertainty as a representation of the uncertainty associated with CPC. The individual uncertainty components are not summed because there is some aspect of double counting with the fit uncertainty. From Table 4 the contribution of the type A, fit uncertainties contribute less than 1 % relative across all concentrations to the overall uncertainty in the measurements.

Table 5. Combined uncertainty in the AE measurements, combined uncertainty in the AE measurements resulting from the type A uncertainties in the CPC measurements and the combined total uncertainty.

Nominal Concentration	Combined Uncertainty u_N/N	Fit Uncertainty $u_{AE}(CPC)/N_{AE}$	Combined Total Uncertainty
120	0.26	0.0041	0.26
500	0.057	0.0010	0.057
3000	0.011	0.0002	0.011
5000	0.006	0.0001	0.006
12 000	0.0035	0.000 05	0.0035

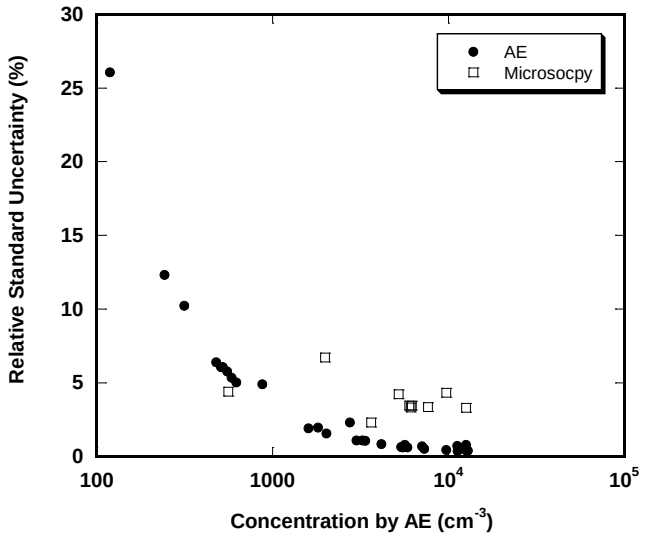

Figure 17. The total sum of the relative standard uncertainty (k = 1)expressed as percent in the AE and microscopy measurements as a function of aerosol concentration.

The combined relative uncertainty for the microscopy measurements shown in Figure 17 is based on the variation in the mean number of particles counted per microscopic field-of-view, the uncertainty in the field-of-view area, the uncertainty in the effective filtration area and the uncertainty in the air flow rate. The field-of-view calculation includes the uncertainty in the SRM 484g SEM pitch standard, and the variation in the actual length measurements made on the SEM stage in both the x and y direction. Table 6 presents a summary of the microscopy uncertainty. This table contains the mean number of particles per field-of-view (FOV), air volume sampled, field-of-view area, total effective filtration area (that is smaller than the filter dimensions), the respective uncertainties, total of standard uncertainty and the expanded uncertainty (k=2) (Taylor and Kuyatt, 1994) .

Table 6. Values and uncertainties obtained for the particle concentration determination by microscopy. Listed are the mean values of the number of particles per field-of-view, the air volume sampled, the area of the field-of-view sampled and the effective particle-covered filter area (4.0811e+08 +/- 0.01678e+08 μm^2) all with their associated uncertainties.

Mean Number Particles per FOV	Uncert.	Air Volume (cm^3)	Uncert. (cm^3)	FOV Area (μm^2)	Uncert. (μm^2)	Conc. (cm^{-3})	Total Uncert. (cm^{-3})	Expanded Uncertainty k=2 (cm^{-3})
12.47	0.52	2.6905e+05	359.1	33.8	0.36	559.8	24.5	49
46.40	3.07	2.808e+05	218.2	33.9	0.36	1986.3	133	266
72.00	2.27	1.2052e+05	241.9	31.9	0.33	7653	260.9	522
14.40	0.58	18324	170.9	33	0.35	9724.1	420.6	841
18.11	0.56	35304	172.6	34.3	0.36	6104.8	202.2	404
17.48	0.56	35304	172.6	32.6	0.34	6205.9	213.6	427
8.18	0.32	18786	159.7	34.1	0.34	5208.2	219.75	439.5
13.64	0.41	12922	109.8	34.1	0.34	12616.1	415.65	831.3
18.26	0.34	60084	510.7	34.1	0.34	3632.6	83.9	167.8
7.55	0.24	15060	128	34.1	0.34	5993.6	206.3	412.6

We have 9 independent measurements of particle concentration by microscopy that span the important concentration range and compare with the associated concentration measurements made by CPC and AE. Table 7 presents the aerosol concentrations measured by the three techniques, microscopy, CPC and AE, and their associated uncertainty over the range of approximately 500 particles/cm^3 to nearly 10 000 particles /cm^3. The two microscopy measurements denoted by (*) found in Table 7 are independent values derived from the same filter, i.e., repeat count determinations from a new set of random fields-of-view. The uncertainty in the CPC results for the variability in the count, the flow rate and the reference CPC that was used as a relative monitor between the test CPC and the AE.

Table 7: Aerosol concentration determined for the same aerosol populations and the associated combined expanded uncertainty (k=2). The CPC determined concentrations are coincidence corrected (type A uncertainty at the 95 % confidence interval).

Concentration by Microscopy (cm^{-3})	Expanded Uncertainty (cm^{-3})	Concentration by AE (cm^{-3})	Expanded Uncertainty (cm^{-3})	Concentration by CPC (cm^{-3})	Type A Uncertainty (cm^{-3})
559.80	49.0	577.01	30.7	583.3	11.2
1986.9	266.4	2880.9	33.9	2835.2	54.0
7653.0	512.4	10428	59.1	9475.5	180.0
9724.1	841.2	9767.0	48.3	8592.2	
6104.8*	404.4	7545.0	53.3	6857.9	130.0
6205.9*	427.2	7545.0	53.3	6857.9	130.0
5208.0	440.0	5649.4	69.9	5303.9	42.4
12616	831.2	12628	99.1	11951	121.0
3632.6	167.8	3011.4	64.7	2859.3	31.4
5993.6	412.6	5516.4	69.5	5397.7	45.0

A plot of these values presented in Figure 18 better illustrates the data. Note that the AE concentration almost always exceeds the CPC value. The spread in the electrospray data is much narrower in part due the elimination of the multiple charge bias and to some extent, better stability in aerosol generation by the electrospray and the ability to correct any aerosol concentration drifts using the continuous CPC monitor (model 3022) that ran through out the experiments (simultaneously for AE and test CPC 3760A).

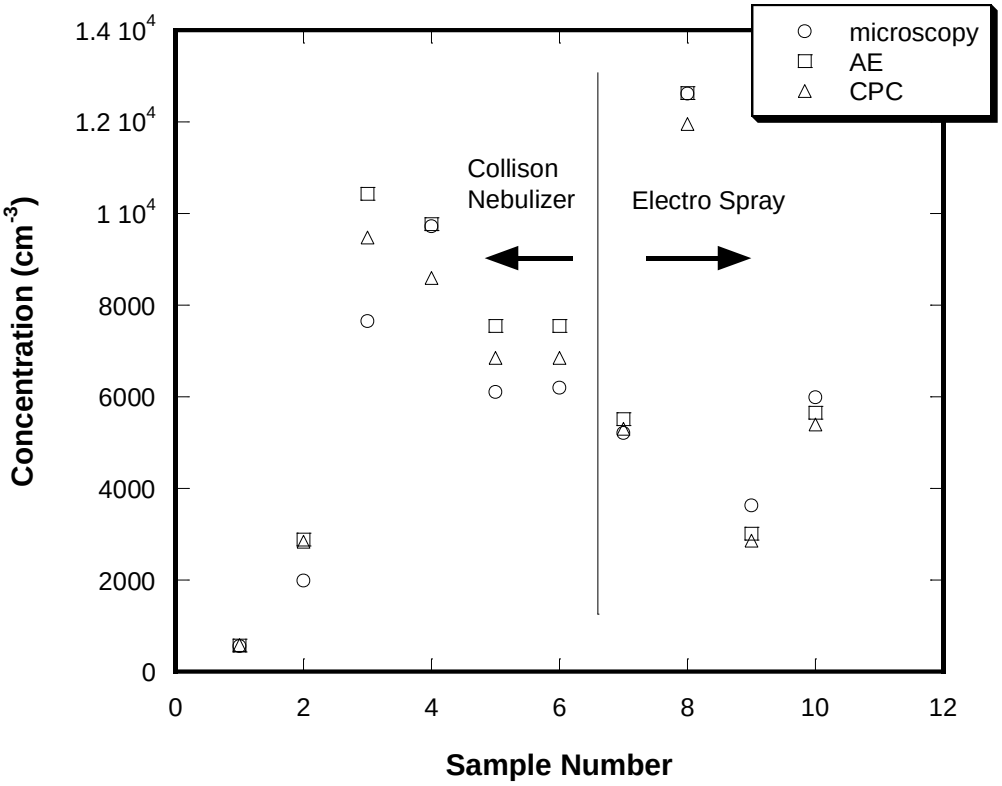

Figure 18. Values found in Table 7 plot for comparison.

Recommendation for Applying the CPC

The bulk of the uncertainty is represented by the calibration with the AE and described above. There are several issues to consider in applying the calibrated CPC. One is the flow rate of the instrument. The flow rate should be measured independently and the uncertainty associated with the measurement and the calibrant taken into account. When sampling an aerosol, at least 10 and preferably 20, 6 s samples should be averaged or the instrument can be set to integrate over a longer sampling period. A single count or just a few count values are not sufficient. The main concern, unless two instruments are sampling simultaneously, is that there are short and long term fluctuations in the aerosol source. The random count uncertainty appears to be slightly larger than expected from Poisson counting. For pure random counting of an aerosol at a concentration of 10 cm^{-3} integrated over 6 s, we would expect to count approximately 10 particles/cm^3 x 150 cm^3 =1500 particles and have an uncertainty of about 3 %. At 100 particles/cm^3 we would expect slightly less than 1 % counting uncertainty.

Model-Calculations of Particle Loss

The calculation of particle losses in various components of a TSI CPC (Model 3760a) is discussed in the appendix. There are four major components in the CPC: (1) entrance tube, (2) saturator, (3) condenser, and (4) conical contraction exit. The working

fluid is n-butanol. The standard sampling flow rate is 1.5 L/min. The saturator temperature is assumed to be at 35 °C. The condenser is operated at 10 °C. The initial aerosol diameter d_p at the entrance tube is 80 nm.

Table 8. Summary of the particle loss mechanisms and estimated loss values.

Mechanism	**Loss (%)**
Inlet diffusion loss	0.11
Diffusion loss in saturator	0.13
Impaction loss in bend	0.001
Thermophoretic loss in condenser	3
Diffusion loss in condenser	3
Loss in nozzle	unknown

Summary and Conclusions

In summary, we have developed a method to measure particle concentration based on NIST traceable electrical current measurements using a calibrated aerosol electrometer. Particle counting by microscopy is utilized as an independent first principle method of determining particle concentration. An electrospray aerosol generator was shown to produce 80 nm aerosol particles with virtually no doublets and thus no multi charge, but with aerosol concentrations spanning the range of interest. We have been able to calibrate the specific CPC used in these experiments and derive a relationship between the uncorrected coincidence CPC response for aerosol concentration to a NIST traceable concentration.

The calibration technique is sensitive enough to reveal a bias in the methods due to multiply charged particles. We think that there is a bias in the AE data collected using the Collison nebulizer and that it is due to particle agglomeration and multiple charging of these agglomerates. SEM micrographs bear this out and the fact that the divergence of the AE-CPC data is most pronounced for high particle concentration is further evidence. By using the electrospray aerosol generator, we were able to greatly reduce agglomeration and thus multiple charge effects that caused a 15 % bias in the measurement. As a consequence, the spread among the three independent methods of measuring aerosol concentration has been reduced as evident in Figure 18. Part of the variation can be due to variation in the aerosol generator. Data is also presented showing a comparison among the three concentration measuring techniques for both Collison nebulizer and electrospray generated aerosol. Model simulations of aerosol loss in the CPC (as a way of estimating the type B uncertainty) indicate that there could be upwards of approximately 6 % loss due to all identified mechanisms. The experimental results indicate that there is very little aerosol loss in the CPC tested.

Acknowledgements

The authors would also like to acknowledge helpful discussions with S. Kaufman, F. Quant, B. Osmondson and G. Sem all current or former TSI employees.

References

Ahn, K-H and Liu, BYH "Particle activation and droplet growth processes in condensation nucleus counter-I. Theoretical background" *J. Aerosol Sc.* 21(2), 249-261. (1990).

Ahn, K-H and Liu, BYH "Particle activation and droplet growth processes in condensation nucleus counter-II. Experimental Study" *J. Aerosol Sc*. 21(2), 263-275. (1990).

Allen, M.D. and Raabe, O.G., "Re-evaluation at Millikan's Oil Drop Data for the Motion of Small Particles in Air," *J. Aerosol Sci*., 13, 537-547 (1982).

Alofs, D.J., Lutrus, C.K., Hagen, D.E., Sem, G.J. and Blesener, J.L. "Intercomparison between commerical condenstaion nucleus counters and an alternating temperature gradient cloud chamber" *Aerosol Sci. and Technol.* 23, 238-249 (1995).

Biermann, A. and Nergman, W. "Measurement of aerosol concentration as a function of size and charge" *Aerosol Sci. and Technol.* 3, 293-304 (1984).

Bird, R.B., Stewart, W.E., and Lightfoot, E.N., *Transport Phenomena*, John Wiley & Sons, New York, 1960.

Chen, D-R. and Pui, D.Y.H., "Numerical and Experimental Studies of Particle Deposition in a Tube with a Conical Contraction – Laminar Flow Regime," *J. Aerosol Sci*., 26, 563-574 (1995).

Cheng, Y.S and Wang, C.S., "Motion of Particles in a Bends of Circular Pipes" *Atmos. Environ.* 15, 301-306 (1981).

Crane, R.I. and Evans, R.L. "Inertial Deposition of Particles in a Bent Pipe" *J.Aerosol Sci.* 8, 161-170 (1977).

Gebhart, Josef, "Optical Direct-reading Techniques: Light Intensity Systems," *Aerosol Measurements: Principles, Techniques, and Applications, (ed. Paul A. Baron and Klaus Willeke),* Wiley-InterScience, Inc., 2001.

DIPPR Data Compilation of Pure Compound Properties Database, V9.02, NIST Standard Reference Data Program #11, NIST, Gaithersburg MD, 1995.

Friedlandler, S.K., *Smoke, Dust, and Haze, Fundamentals of Aerosol Dynamics*, 2nd ed., Oxford University Press, New York, 2000.

Fuchs, N.A., *The Mechanics of Aerosols*, Dover Publications, Inc. New York, 1989.

Green, B., Ratnikov, B., Stofer, D. and Aicholtz, P. " How the Latex Sphere Challege Impacts on Submicron Membrane Ratings." Presented at the annual meeting of the American Filtration Society (1991).

He, L., Alling, D., Popkin, T., Shapiro, M., Alter, H. and Purcell, R. "Determining the Size of Non-A, Non-B Hepatitis Virus by Filtration*." J. Infect. Dis*. 156 No. 4, 636 (1987).

Kesten, J., Reineking, A. and Portendorfer, J. " Calibration of a TSI 3025 ultrafine condensation particle counter" *Aerosol Sci. and Technol*. 15, 107-111 (1991).

Liu, P.S.K. and Deshler, T. "Causes of concentration differences between a scanning mobility particle sizer and a condensation particle counter" *Aerosol Sci. and Technol*. 37, 916-923 (2003).

Liu, B.Y.H. and Pui, D.Y.H. " A Submicron Aerosol Standard and Primary, Absolute Calibration of the Condensation Nuclei Counter" *J. Coll. Interf. Sci.* 47 No. 1, 156-171 (1974).

Liu, B.Y.H., Pui, D.Y.H., Hogan, A.W., and Rich, T.A. "Calibration of the Pollak Counter with Monodisperse Aerosols" *J. Appl. Meteorology* 14 (1), 46-51 (1975).

Liu, B.Y.H., Pui, D.Y.H., McKenzie, R.L., Agarwal, J.K., Jaenicke, R., Pohl, F.G., Preining, O., Reischl, G., Szymanski, W. and Wager, P.E. "Intercomparison of different "absolute" instruments for measurement of aerosol number concentration" *J. Aerosol Sci.* 13(5), 429-450 (1982).

Li W. and Davies, E.J., "Measurement of the Thermophoretic Force by Electrodynamic Levitation: Microspheres in Air," *J. Aerosol Sci*., 26, 1063-1083 (1995).

Liu, B.Y.H. presentation American Association for Aerosol Research Annual Conference (2004).

Liu, B.Y.H. private communication (2005).

McGrattan, K.B. and Forney, G.P., "Fire Dynamics Simulator – User's Manual," *NISTIR 6469*, U.S. Department of Commerce, Washington, D.C., January 2000.

Osmondson, B. and Sem, G. private communication (2004).

Pisani, J.F. and Thomas, G.H., "Coincidence Errors in Automatic Particle Counters," *J. Phys E:* Scientific Instruments 4, 59-61, (1971).

Reid, R.C., Prausnitz, J.M., and Poling, B.E., *The Properties of Gases and Liquids*, 4th ed., McGraw-Hill, Inc., New York, 1987.

Snedecor, G.W. and Cochran, W.G. Statistical Methods. The Iowa State University Press, Ames, Iowa 6th ed. pp.159-160. (1967).

Stolzenburg, M.R. and McMurry, P.H. "An ultrfine aerosol condensation nucleus counter" *Aerosol Sci. and Technol*. 14, 48-65 (1991).

Taylor, BN and C.E. Kuyatt "Guidelines for Evaluating and Expressing the Uncertainty of NIST Measurement Results. *NIST Technical Note 1297* (1994)

TSI model 3760A instrument manual.

Van der Meulen, Plomp, A., Oeseburg, F., Buringh, E., van Aalst, R.M., Hoevers, W., "Intercomparison of Optical Particle Counters Under Conditions of Normal Operation," *Atmospheric Environment* 14, 495-499, (1980).

Ye, Y. and Pui, D.Y.H., "Particle Deposition in a Tube with an Abrupt Contraction," *J. Aerosol Sci*. 21, 29-40 (1990).

Waldmann, L. and Schmitt, K.H., "Thermophoresis and Diffusiophoresis of Aerosols," in Chapter VI, *Aerosol Science*, Davies, C.N. (ed.), Academic Press, New York, 1966.

Zhang, Z. and Liu, B.Y.H. "Performance of TSI 3760 condensation nuclei counter at reduced pressures and flow rates" *Aerosol Sci. and Technol*. 15, 228-238 (1991).

Zhang, Z. and Liu, B.Y.H. "Dependence of the TSI 3020 condensation nucleus counter on pressure, flow rates and temperature" *Aerosol Sci. and Technol*. 13, 493-504 (1990).

APPENDIX

Calculated Estimates of Particle Loss in the 3760a Condensation Particle Counter

Entrance tube

The entrance tube has a length L and a diameter d_e. Based on the volumetric airflow Q of 1.5 L/min, the average velocity V_{tube} in the tube was calculated to be 0.79 m/s. The Reynolds number, $Re = \frac{d_e V_{tube} \rho}{\mu}$, equals 326, where ρ and μ are the density and viscosity of air evaluated at 295 K. The flow is laminar. Since there is no temperature gradient in the tube (assuming isothermal at 295 K and 101×10^3 Pa), thermophoresis is not present. Only diffusion loss to the tube wall is considered. For laminar flow, the diffusion loss in the entrance tube can be estimated using the following two equations (Friedlander, 2000):

For $\Pi = \pi DL / Q < 0.02$,

$$\text{Loss} = 1 - \frac{n_2}{n_1} = 2.56\,\Pi^{2/3} + 1.2\,\Pi + 0.1767\,\Pi^{4/3} + \cdots \qquad \text{(A1)}$$

where D is the diffusion coefficient, n_1 and n_2 are the inlet and outlet number concentrations respectively.

For $\Pi = \pi DL/Q > 0.02$,

$$\text{Loss} = 1 - \frac{n_2}{n_1} = 1 - 0.819\exp(-3.66\,\Pi) + 0.095\exp(22.3\,\Pi) + 0.0325\exp(-57.0\,\Pi) + \cdots \qquad \text{(A2)}$$

The diffusion coefficient can be calculated using the Stokes-Einstein equation (Friedlander, 2000):

$$D = \frac{kT}{f} \qquad \text{(A3)}$$

where k is the Boltzmann's constant (= 1.38066×10^{-23} J/K), T is the absolute temperature, and f is the friction coefficient, which can be calculated by:

$$f = \frac{3\pi\mu d_p}{C} \qquad \text{(A4)}$$

where the slip correction factor C is given by

$$C = 1 + \frac{2 l_p}{d_p}\left[A_1 + A_2 \, exp\left(\frac{-A_3 \, d_p}{l_p} \right) \right] \tag{A5}$$

where l_p is the mean free path of the gas molecules and A_1(= 1.257), A_2 (= 0.400), and A_3 (= 0.55) are constants. The mean free path was calculated using the following two equations (Bird *et al*., 1960)

$$d = \sqrt{\frac{2\sqrt{m k T}}{3\pi^{\frac{3}{2}} \mu}} \tag{A6}$$

$$l_p = \frac{1}{\sqrt{2}\,\pi d^2 n} \tag{A7}$$

where d is the molecular diameter, m is the molecular mass, and n is the molecular concentration (number of molecules per unit volume).

Figure A1, shows the results of the calculation for diffusion loss as a function of aerosol diameter. Under the above operational conditions of the entrance tube to the CPC, the diffusion loss is estimated to be **0.11 %** for the 80 nm particles.

Saturator

Since the aerosol entering the saturator has a diameter of 80 nm, the particles will follow the flow path. Therefore, it is expected that there would be negligible inertial deposition of particles on the insert. In addition, there should be no particle loss due to thermophoresis because the saturator walls and the insert are maintained at a temperature higher than that of the bulk flow through the saturator.

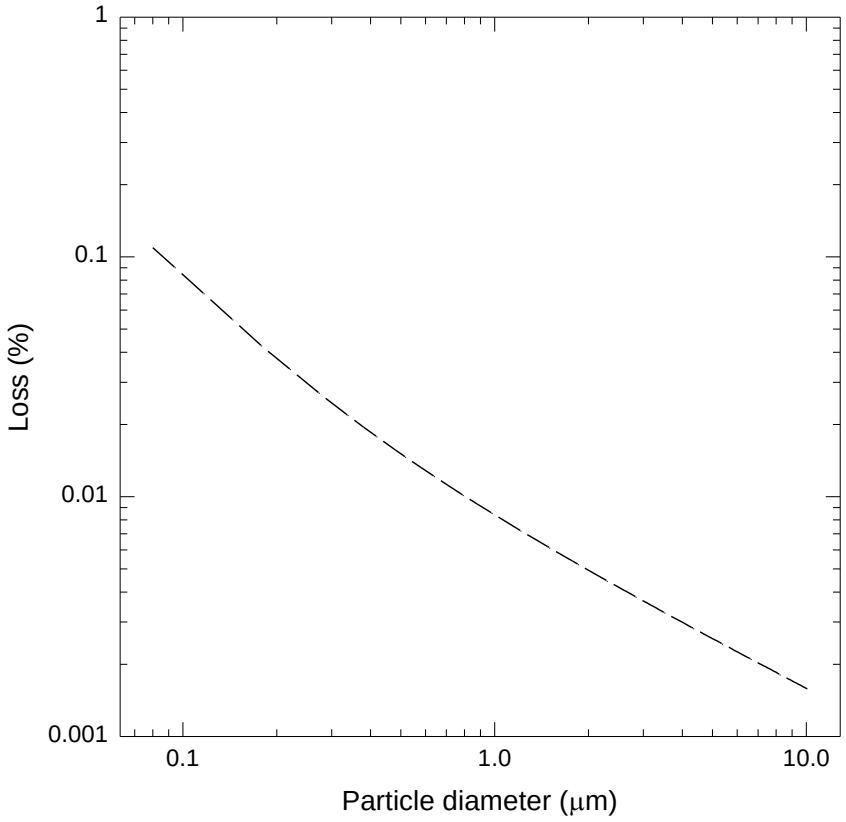

Figure A1. Diffusion loss as a function of particle diameter in the entrance tube.

A detailed analysis of the flow and temperature fields is needed for the calculation of the diffusion loss. In this regard, the NIST Fire Dynamics Simulator (FDS) computational fluid dynamics code (McGrattan and Forney, 2000) may be used to estimate the diffusion loss by assuming the aerosol as "point" particles. However, for a zero-order analysis without considering the effect of the insert, the diffusion loss was assessed using the formula given in Fuchs (1989) for a laminar flow through a channel with parallel plane walls.

$$\text{Loss} = 1 - \frac{n_2}{n_1} = 1 - 0.9149\exp\left(-1.885\,\Pi\right) + 0.0592\exp\left(-22.3\Pi\right) + 0.0258\exp\left(-151.8\Pi\right) \tag{A8}$$

where in this case $\Pi = \dfrac{D\,L}{h^2\,V_{channel}}$, L is the length of the channel, h is the half height of the channel, and $V_{channel}$ is the average velocity through the channel.

Figure A2 shows the diffusion loss as a function of particle diameter calculated using Eq. (A8) at 295 K and 101×10^3 Pa. For 80 nm particles, the loss is estimated to be **0.13 %**.

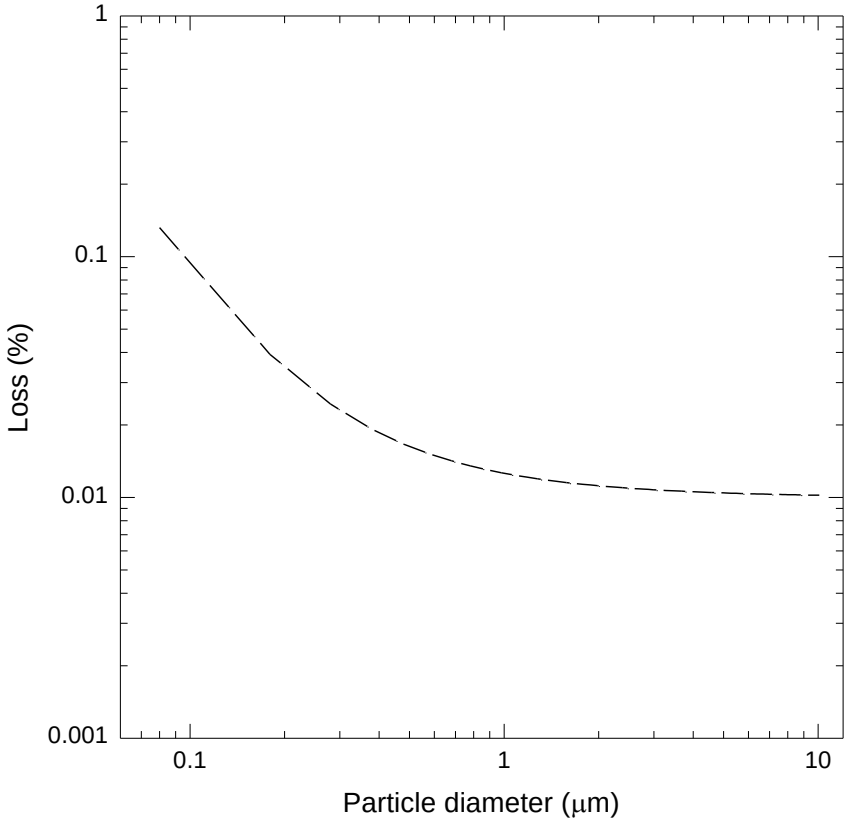

Figure A2. Diffusion loss as a function of particle diameter in the saturator with no insert.

Impaction in the turn

There is a chance of particle loss in the right-angle bend that the aerosol follows from the saturator to the condenser. Assuming 80 nm particles and velocities of 17.86 cm/s following Cheng and Wang, 1981; Crane and Evans, 1977, we found less than **0.001%** loss due to impaction. This is reasonable given the particle are so small and have little inertia.

Condenser

The flow is laminar, and the entrance length L_e for the flow to be fully developed was estimated to be $4R$ (Zhang and Liu, 1990).

Due to the temperature gradient established within the condenser tube, thermophoresis has to be examined. The thermophoretic velocity of n-butanol aerosol can be estimated

using the formulations given in Li and Davis (1995). The thermophoretic force, $\vec{K}$, is given by

$$\vec{K} = -9\pi \frac{\mu^2 a}{\rho T} \left(\frac{1}{1 + 3C_m \frac{l_p}{a}} \right) \left(\frac{\frac{k_f}{k_s} + C_t \frac{l_p}{a}}{1 + 2\frac{k_f}{k_s} + 2C_t \frac{l_p}{a}} \right) \vec{\nabla} T_\infty \tag{A9}$$

where μ is the viscosity of the gas (in this case, air), a is the particle radius, ρ is the gas density, k_f is the thermal conductivity of the gas, k_s is the thermal conductivity of the particle, $\vec{\nabla} T_\infty$ is the temperature gradient at large distance from particle.

$$C_t = \frac{15}{8} \left(\frac{2 - \alpha_t}{\alpha_t} \right) \tag{A10}$$

$$C_m = \frac{2 - \alpha_m}{\alpha_m} \tag{A11}$$

$$\alpha_t = \frac{E_i - E_r}{E_i - E_w} \tag{A12}$$

$$\alpha_m = \frac{M_i - M_r}{M_i - M_w} \tag{A13}$$

where α_t is the thermal accommodation coefficient, E_i is the average incident molecular energy flux at a point on the surface, E_r is the average energy flux for molecules leaving the surface, E_w represents the energy flux which would be emitted if the molecules left in Maxwellian equilibrium, α_m is the momentum accommodation coefficient or reflection coefficient for the tangential component of the momentum, M_i is the average incident molecular momentum flux at a point on the surface, M_r is the average momentum flux for molecules leaving the surface, and M_w represents the momentum flux which would be emitted if the molecules left in Maxwellian equilibrium.

For this analysis, a reasonable approximation for the accommodation coefficients (α_t, α_m) is a value of 1. Therefore, $C_t = 15/8$ and $C_m = 1$.

For the calculations, the thermophysical properties of air and n-butanol were obtained from DIPPR database (DIPPR, 1995). The viscosity of air (in N s/m^2) is given by

$$\mu = \frac{1.425 \times 10^{-6} T^{0.5039}}{1 + \frac{108.3}{T}} \tag{A14}$$

The thermal conductivity of air (in W/m K) is calculated using

$$k_f = \frac{3.1417\times10^{-4}T^{0.7786}}{1-\frac{0.7116}{T}+\frac{2121.7}{T^2}} \tag{A15}$$

The thermal conductivity (in W/m K) of liquid n-butanol is given by

$$k_s = 0.2136 - 2.034\times10^{-4}T \tag{A16}$$

The mean free path of air can be calculated using the following equation from Allen and Raabe (1982):

$$l_p = l_o\left(\frac{T}{T_o}\right)\left(\frac{P_o}{P}\right)\left(\frac{1+\frac{110.4}{T_o}}{1+\frac{110.4}{T}}\right) \tag{A17}$$

where l_o (= 0.0673 μm) is the mean free path of air at reference T_o (= 296.15 K) and P_o (= 1.0133×10^5 Pa). The density of air is calculated using the ideal gas law.

The thermophoretic velocity can be obtained from a force balance given below.

$$m\frac{d\vec{V}_t}{dt} = \vec{K} - \frac{6\pi\mu a}{C}\vec{V}_t \tag{A18}$$

where m is the mass of the particle. If we assume the relaxation time of the particle compared to its drift time is small, the thermophoretic velocity is

$$\vec{V}_t = \frac{C\vec{K}}{6\pi\mu a} \tag{A19}$$

To calculate the thermophoretic velocity, one needs to know the temperature gradient in the condenser. A direct numerical simulation (DNS) of the steady-state temperature profile in the condenser was carried out using the FDS code (McGrattan and Forney, 2000). Since the code utilizes a Cartesian coordinate system, the shape of the circular condenser was approximated using rectangular steps. The number of grids used in the simulation were 12×12×60. Figure A3 shows the temperature profiles in the condenser tube. In the figure, z and r are the axial and radial coordinates, respectively. From the temperature profile, the maximum $\left|\vec{\nabla}T_\infty\right|$ was estimated to be in the order of 2×10^4 K/m at z/R = 0.5. Figure A4 shows the magnitude of calculated thermophoretic velocity as a

function of particle diameter with three values of $\left|\vec{\nabla} T_{\infty}\right|$. The calculations were performed using $T = 295$ K, $P = 101\times10^3$ Pa.

The importance of the thermophoresis can now be qualitatively assessed based on the above analysis. For the particle size range indicted in Figure A4, $V_{condenser}$ is at least three order of magnitude higher than V_t. The residence time t_R in the condenser tube is $L/V_{condenser} = 0.41$ s. However, thermophoresis is not likely to occur within the entire condenser because based on Figure A3 $\left|\vec{\nabla} T_{\infty}\right|$ is essentially zero at $z/R \geq 17$. Therefore, a corrected residence time τ of $17R/V_{condenser} = 0.22$ s was used to assess particle loss due to thermophoresis. The *average* distance (d_t) that the particle travels within τ as a result of thermophoresis is $\left|\vec{V}_t\right| \times \tau$. If we assume that the particles within a distance of d_t from the condenser wall will be deposited on wall within τ and that *the particle flux profile* (F) *is uniform*, the deposition efficiency of the aerosol particles in the condenser tube can be calculated as follows (Ye and Pui, 1990):

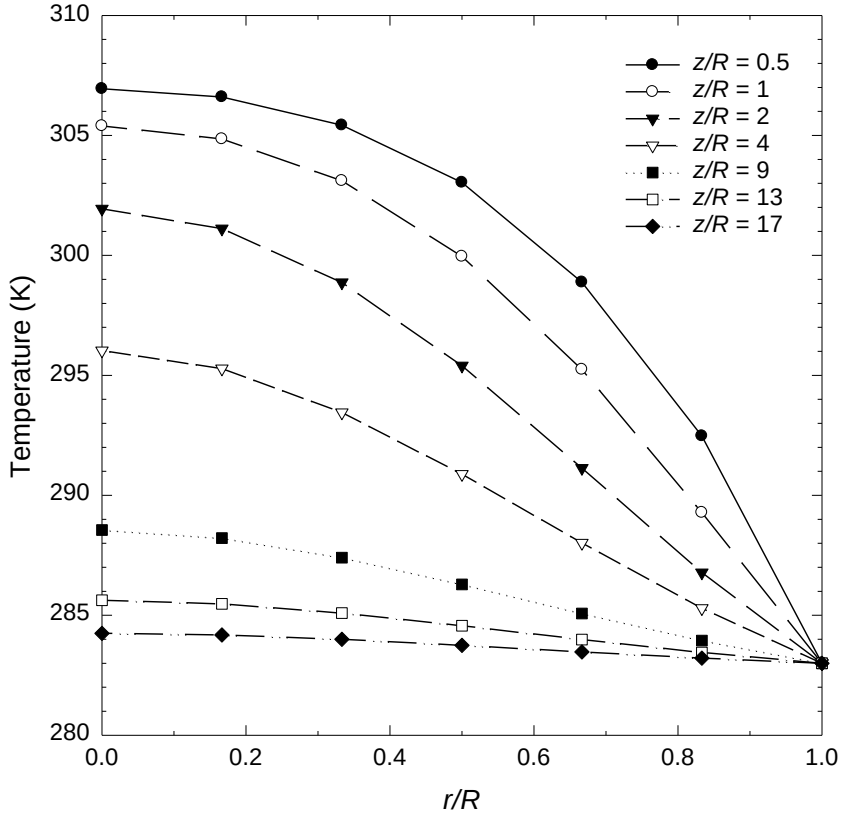

Figure A3. Steady-state temperature profiles in the condenser tube.

$$\eta = \frac{\int_{d_c/2-d_t}^{d_c/2} F\,r\,dr}{\int_{0}^{d_c/2} F\,r\,dr} \tag{A20}$$

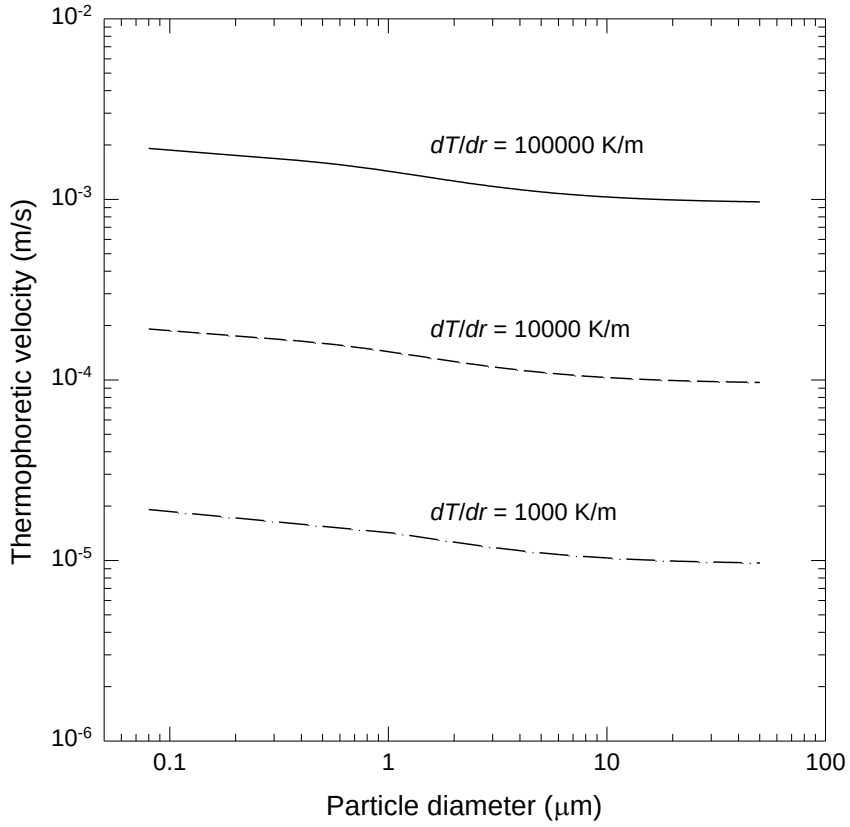

Figure A4. Thermophoretic velocity and particle loss as a function of particle diameter

Upon integration with $F = \text{constant} \neq F(r)$

$$\eta = \left[1 - \left(\frac{d_c - 2\,d_t}{d_c}\right)^2\right] \tag{A21}$$

Figure A5 shows the particle loss due to thermophoresis as a function of particle diameter at three temperature gradients.

The diffusiophoretic velocity (V_{sph}) is estimated based on the following formulae reported in Waldmann and Schmitt [1966]:

$$V_{sph} = -\sigma_{12}\, D_{12}\, \vec{\nabla} y_{1\infty} \tag{A22}$$

where σ_{12} is the diffusion slip factor, D_{12} is the diffusion coefficient of butanol vapor in air and $\vec{\nabla} y_{1\infty}$ is the concentration (mole fraction) gradient of butanol at large distance from the aerosol particle. The diffusion slip factor is given by:

$$\sigma_{12} = \frac{m_1 - m_2}{m_1 y_1 + m_2 y_2 + \sqrt{m_1 m_2}} \tag{A23}$$

where m is the molecular mass, y is mole fraction, and the subscripts 1 and 2 represent butanol and air respectively.

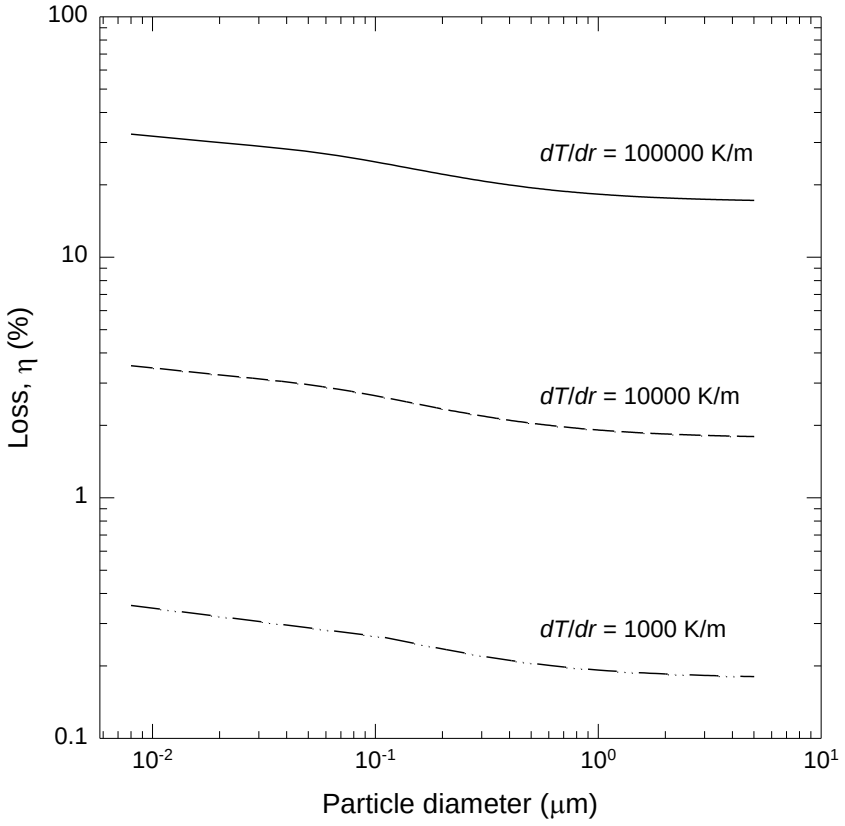

Figure A5. Particle loss due to thermophoresis as a function of particle diameter at various temperature gradients.

A direct numerical simulation (DNS) of the steady-state butanol vapor concentration profile in the condenser was also carried out using the FDS code. The concentration at the wall boundary was assumed to be at the saturation value. Figure A6 shows the concentration profiles in the condenser. From the concentration profile, $\left|\vec{\nabla} y_{1\infty}\right|$ was

estimated to be in the order of 10 m^{-1}. The magnitude of calculated diffusiophoretic velocity with $\left|\vec{\nabla} y_{1\infty}\right| \approx O(10\ m^{-1})$, $D_{12} \approx O(10^{-5}\ m^2/s)$ [Reid *et al.*, 1987], and $\sigma_{12} \approx O(1)$, is $\approx O(10^{-4}$ m/s). The diffusiophoretic velocity is in the same order of magnitude as the thermophoretic velocity, and it is expected that the loss due to diffusiophoresis is comparable to that due to thermophoresis.

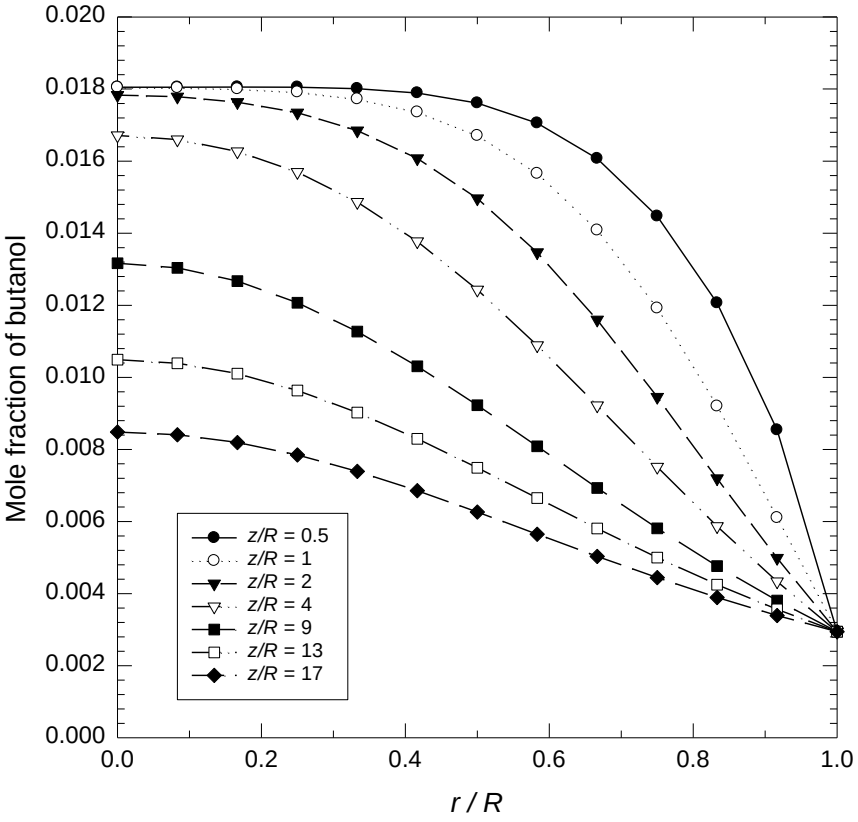

Figure A6. Steady-state concentration profiles in the condenser tube.

The formulation described in the Entrance-tube section above was used to estimate the diffusion loss in the the condenser, the properties of air was used in the calculations for simplicity. Figure A7 shows the diffusion loss as a function of particle diameter at a characteristic condenser. Because the butanol vapor concentration in air is not high (see Figure A6) in temperature of 296 K (average temperature between the condenser wall and the inflow) and 101×10^3 Pa. Over this size range, the diffusion loss is relatively small compared to the losses due to thermophoresis and diffusiophoresis.

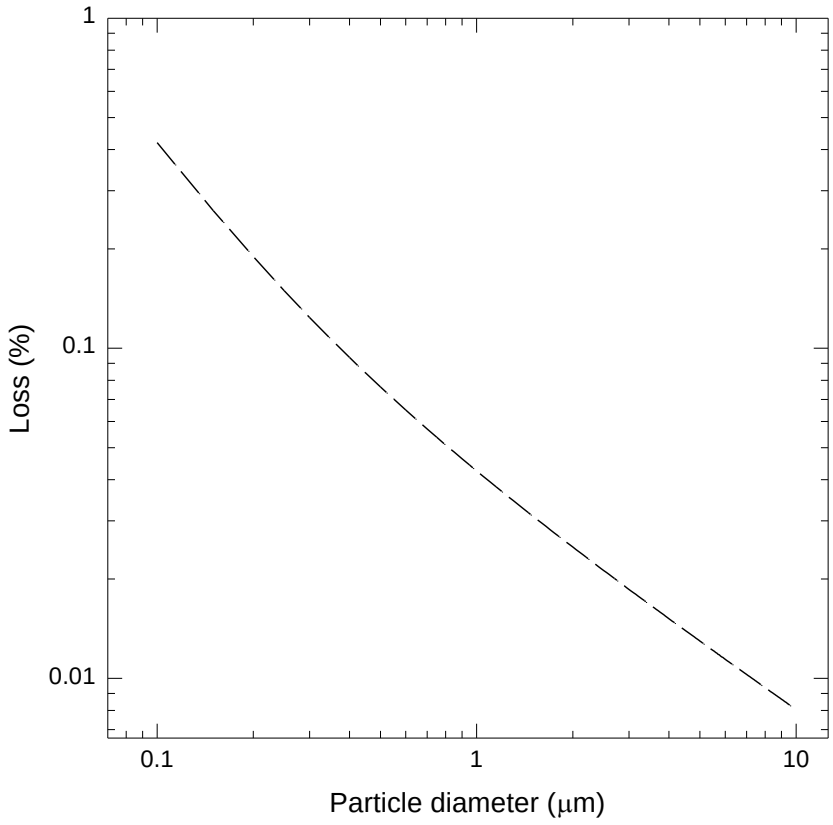

Figure A7. Diffusion loss in the condenser as a function of particle diameter.

Conical Contraction

The exit of the condenser in the current CPC has a configuration similar to the conical contraction that was used in the numerical study of Chen and Pui (1995). The loss at the condenser exit was estimated using the correlation obtained from their study. The empirical equation is given by:

$$\eta = \left[1 - \left(\frac{D_o}{D_i}\right)^2\right]^2 \times \left[0.882 + 0.0272\, X^{0.5} - 8.272\, X^{0.5} \exp\left(-3.627\, X^{0.5}\right)\right]^2 \quad \text{(A24)}$$

where D_i is the diameter of the contraction inlet, D_o is the diameter of the contraction outlet, and $X = St / St(50\ \%)$. St is the Stokes number and is defined as

$$St = \frac{\rho_p\, d_p^2\, C V_m}{9 \mu\, D_o} \quad \text{(A25)}$$

where V_m is the average velocity at the inlet and ρ_p is the mass density of the particle, and

$$St(50\%) = 0.235\left(\frac{D_i}{D_o}\right)^{0.61}(\sin\Theta)^{-1.119} \quad \text{(A26)}$$

where Θ is the contraction angle. Figure A8 is the geometry of the conical contraction used in the calculation. Figure A9 shows the loss as a function of aerosol diameter. The calculations were obtained using the following equation for liquid density of n-butanol (DIPPR, 1995).

$$\rho_p = \frac{0.965 \times 74.12}{0.2666^{1+\left(1-\frac{T}{563.05}\right)^{0.24419}}} \quad \text{(A27)}$$

From Figure A9, there is >80% loss for particles 5 μm and larger. Experimentally, the loss was found to increase with particle size (Chen and Pui, 1995). The above analysis is based on a fully developed flow at the conical contraction inlet. The current CPC has a short entrance length to the conical contraction, and it is likely that the inlet flow may not be fully developed. In addition, the correlation (Eq. 22) has only been experimentally validated using aerosol size ranged from 3 μm to 16 μm, a contraction ratio (D_i/D_o) of 2, a Reynolds number of 817, and three contraction angles (75°, 45°, 15°).

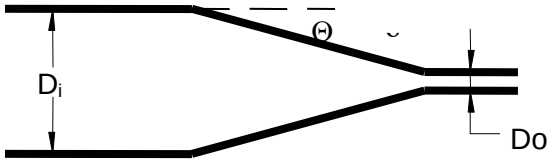

Figure A8. Nozzle configuration.

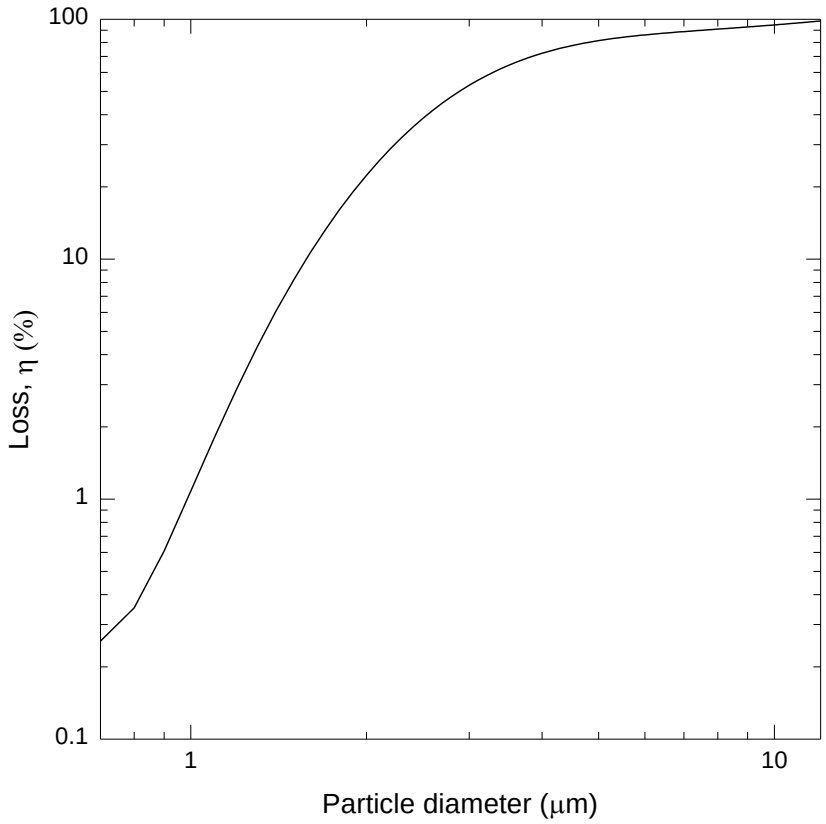

Figure A9. Particle loss in nozzle as a function of particle size.

Given the loss curve, one needs to determine the droplet size to find the effective loss due to the nozzle constriction. The CPC was dried out so that no alcohol vapor was present in the instrument. Then the pulse height response of the optical detector was determined using aerosolized mondisperse PSL. Particles from 0.5 μm to 7 μm in diameter were employed. Particles larger than 7 μm could not be transported to the sensing region of the instrument. Then the CPC was filled with alcohol and returned to normal operating conditions. The pulse height was determined for 80 nm PSL – alcohol droplets. The size of these droplets appears to be greater than 10 μm diameter based on an extrapolation fit to the existing PSL data (see Figure A10). If the droplets are >10 μm, then the droplets should be removed at > 90 % efficiency according to Chen and Pui. Comparison with AE and microscopy indicate this is not the case. There is a remaining question with regard to understanding loss in the nozzle. Either there is some error in the Chen and Pui work or there is an order of magnitude error in the droplet measurement that is unlikely. We will not further explore this interesting problem due to time constraints.

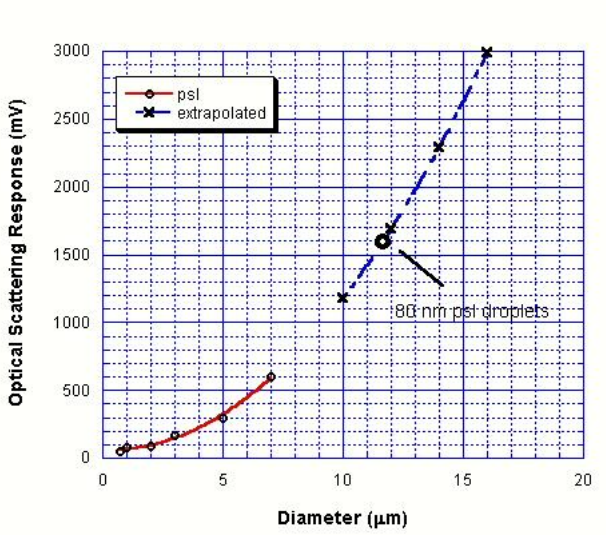

Figure A10. Plot of CPC optical scattering response as a function of particle diameter. The top part of the curve is extrapolated and the bottom is fitted to polystyrene spheres.

Total Losses

Based on the losses due to the individual components in the CPC, the following equation can be derived to assess the total loss η_{total} of the system:

$$\eta_{total} = 1 - \prod_{i=1}^{n} [1 - \eta_i] \qquad \text{(A28)}$$

where η_i is the loss of component i (*e.g.*, entrance tube) and n is the total number of components (in this case, the entrance tube, saturator, condenser, and conical contraction) in the CPC. Based on the above estimations and Eq. 28, the dominant loss appears to be in the conical contraction. However, experiments are needed to validate the estimation in the contraction nozzle. The determined losses are summarized for diffusion in the inlet 0.11%, diffusion loss in the saturator 0.13%, impaction loss in the bend <0.001%, and diffusion and thermophoretic loss in condenser 3%, respectively. This leads to an overall 6% calculated loss in the CPC.